

HINDRANCE OF THE MYOSIN POWER STROKE POSED BY THE PROXIMITY TO
THE TROPONIN COMPLEX IDENTIFIED USING A NOVEL LRET
FLUORESCENT NANOCIRCUIT

Pilar G. Coffee Castro-Zena

Thesis Prepared for the Degree of:

MASTER OF SCIENCE

UNIVERSITY OF NORTH TEXAS

May 2007

APPROVED:

Douglas Root, Major Professor
Kent D. Chapman, Committee Member
Rebecca Dickstein, Committee Member
Arthur J. Goven, Chair of the Department of
Biological Sciences
Sandra L. Terrell, Dean of the Robert B.
Toulouse School of Graduate Studies

Coffee Castro-Zena, Pilar G. Hindrance of the Myosin Power Stroke Posed by the Proximity to the Troponin Complex Identified Using a Novel LRET Fluorescent Nanocircuit. Master of Science (Biochemistry), May 2007, 49 pp., 1 table, 12 illustrations, references, 53 titles.

A novel luminescence resonance energy transfer (LRET) nanocircuit assay involving a donor and two acceptors in tandem was developed to study the dynamic interaction of skeletal muscle contraction proteins.

The donor transmits energy relayed to the acceptors distinguishing myosin subfragment-1 (S1) lever arm orientations. The last acceptor allows the detection of S1's bound near or in between troponin complexes on the thin filament. Additionally, calcium related changes between troponin T and myosin were detected.

Based on this data, the troponin complex situated every 7 actin monomers, hinders adjacently bound myosins to complete their power stroke; whereas myosins bound in between troponin complexes undergo complete power strokes.

Copyright 2007

by

Pilar G. Coffee Castro-Zena

ACKNOWLEDGEMENTS

I wish to acknowledge Dr. Douglas Root for his enlightened mentoring and continuous support. Additionally, special thanks to Dipesh Patel for providing Cy7-troponin T.

This work was supported by grants from the National Institutes of Health and the National Institute of Arthritis and Musculoskeletal and Skin Diseases.

TABLE OF CONTENTS

| | Page |
|--|------|
| ACKNOWLEDGEMENTS | iii |
| LIST OF TABLES | vii |
| LIST OF ILLUSTRATIONS..... | viii |
| LIST OF ABBREVIATIONS..... | ix |
| Chapter | |
| 1. INTRODUCTION | 1 |
| 1.1 Acto-Myosin Components and Muscle Contraction | |
| 1.2 The Lever Arm Model and Myosin Subfragment-1 | |
| 1.3 Transition State Analogs of ATP Hydrolysis by Myosin | |
| 1.4 Objectives | |
| 2. EXPERIMENTAL MATERIALS AND METHODS | 12 |
| 2.1 Preparation of Myosin Subfragment-1 by Papain Treatment and Endogenous RLC Heat Extraction | |
| 2.2 DTNB Purification and Terbium Chelate Conjugation of RLC | |
| 2.3 CS124-Tb-RLC Exchange to S1 and Labeling Ratio by Terbium Titration | |
| 2.4 Tropomyosin- α Purification and Cy7 Labeling | |
| 2.5 Nanocircuit Assay in Solution | |
| 2.6 Nanocircuit LRET Measurements | |
| 2.7 Data Analysis: Single and Double Exponential Fitting of Decay Curves | |
| 3. EXPERIMENTAL DESIGN | 22 |
| 3.1 Nanocircuit Components | |
| 3.2 Theory of Luminescence Resonance Energy Transfer (LRET) | |
| 4. RESULTS | 26 |
| 4.1 FRET Strategy: No Cross Contamination Between Donor and Last Acceptor | |

| | | |
|-----|---|----|
| 4.2 | Nanocircuit LRET Distances Compared to X-ray Diffraction and Other FRET Measurements of the Myosin Lever Arm to the Nucleotide Binding Site | |
| 4.3 | Calcium Induced Thin Filament Structural Changes Detected by the Nanocircuit. | |
| 4.4 | Post-Power Stroke Lever Arm Conformations Detected on Myosins Bound Close to Cy7-Tropomyosin α and Far Away From the Troponin Complex. Pre-Power Stroke Conformations Detected on Myosins Bound Close to Cy7-Troponin T | |
| 5. | DISCUSSION | 35 |
| 5.1 | Steric Hindrance on Lever Arm Rotation Model: Myosins bound Proximally to the Troponin Complex have a Lever Arm biased towards Pre-Power Stroke State whereas Myosins bound in between the Troponin Complex have Lever Arms in Post-Power Stroke States | |
| 5.2 | What Value Does a Prevention of a Power Stroke near a Troponin Complex Have? | |
| 5.3 | Transition State Analogs Aluminum and Beryllium Fluoride behave similarly causing Pre-Power Stroke Conformations when observed with Troponin T and Post-Power Stroke Conformations when observed from Tropomyosin | |
| 5.4 | Cooperativity of Activation | |
| 5.5 | Calcium Induced Thin Filament Structural Changes Detected by Nanocircuit | |
| 5.6 | Other Possible Applications of the Fluorescent Nanocircuit | |
| 5.7 | Conclusions | |
| | REFERENCES..... | 45 |

LIST OF TABLES

| | Page |
|---|------|
| 1. Fluorescent nanocircuit analysis of lever arm position | 30 |

LIST OF ILLUSTRATIONS

| | Page |
|---|------|
| 1. The sarcomere and components | 3 |
| 2. Myosin subfragment-1 | 5 |
| 3. Papain digested subfragment-1 and RLC heat removal | 13 |
| 4. RLC purification and labeling | 14 |
| 5. CS 124-Tb-RLC exchange into S1 and labeling efficiency | 16 |
| 6. Tropomyosin α | 18 |
| 7. Components of the nanocircuit relay | 23 |
| 8. Nanocircuit: no cross contamination between donor and last acceptor | 27 |
| 9. Emission spectra of complete nanocircuit assay with troponin T label | 28 |
| 10. Lever arm positions and calcium effect | 31 |
| 11. Luminescence decay curves | 34 |
| 12. Hindrance of lever arm rotation model | 37 |

LIST OF ABBREVIATIONS

| Abbreviation | Meaning |
|-----------------------|--|
| ADP | Adenosine diphosphate |
| AlF ₄ -ADP | Aluminum fluoride- Adenosine diphosphate |
| BeF _x -ADP | Beryllium fluoride- Adenosine diphosphate |
| CS124 | Carbostyryl 124, 7-amino-4-methyl-2(1 <i>H</i>)-quinolinone |
| Cy3, Cy5 | Cyanine dye trademark names |
| DMSO | Dimethyl sulfoxide |
| DTNB | 55'-dithiobis-(2-nitrobenzoic acid) (Ellman's reagent) |
| DTPA | Diethylene triamine pentaacetic acid |
| DTT | Dithiothreitol |
| <i>E</i> | Efficiency of energy transfer |
| E 64 | <i>Trans</i> -Epoxysuccinyl-L-leucylamido(4-guanidino)butane |
| FPLC | Fast protein liquid chromatography |
| FRET | Fluorescence resonance energy transfer |
| <i>J</i> | Overlap integral |
| κ^2 | Orientation factor |
| LRET | Luminescence resonance energy transfer |
| η^{-4} | Refractive index |
| Φ_D | Emission intensity of donor |
| R_i | Distance between donor/acceptor pair |
| RLC | Regulatory light chain of myosin |
| R_0 | Critical transfer distance |
| S-1 | Subfragment 1 of myosin |
| Tb ³⁺ | Terbium ion |
| τ_d | Lifetime of the donor alone |
| τ_{da} | Lifetime of the sensitized emission of the acceptor in presence of donor |
| Tm | Tropomyosin |
| Tn C | Troponin C |
| Tn I | Troponin I |
| Tn T | Troponin T |

CHAPTER 1

INTRODUCTION

1.1 Acto-Myosin Components and Muscle Contraction

Myosins comprise a large superfamily of motor proteins that couple movement along actin filaments with the hydrolysis of ATP. There are about 20 classes of myosins classified as such on the basis of amino acid sequence differences in their ATP-hydrolyzing motor domains with additional differences among classes found in the structure of their tail domains. Myosins II in particular are studied for their role in muscle contraction. The myosin II molecule is comprised of two heavy chains and two light chains. The globular motor domain of each heavy chain catalyzes the hydrolysis of ATP and interacts with the actin thin filament. Two light chains, the essential light chain and the regulatory light chain wrap around the neck region of each heavy chain. The tail domains of myosin II heavy chains contain heptads repeat sequences involved in dimerization in which several tails interact to form a rod-like α -helical coiled coil responsible for the formation of the thick filaments.

Skeletal muscle is also referred to as striated muscle due to the consistent, highly ordered interdigitating arrangement of the thin and thick myofilaments into sarcomeres (Fig.1A). The sarcomere is the fundamental, functional unit of skeletal muscle. The thin filaments consist predominantly of G-actin, a 42 KDa protein. G-actin monomers polymerize end to end in the sarcomere to form filamentous F-actin, and two F-actin strands coil around each other in a double helical array in a manner analogous to two pearl necklaces wrapped together. Tropomyosin, a rope-like regulatory protein coils around F-actin covering actin active binding sites for myosin. At

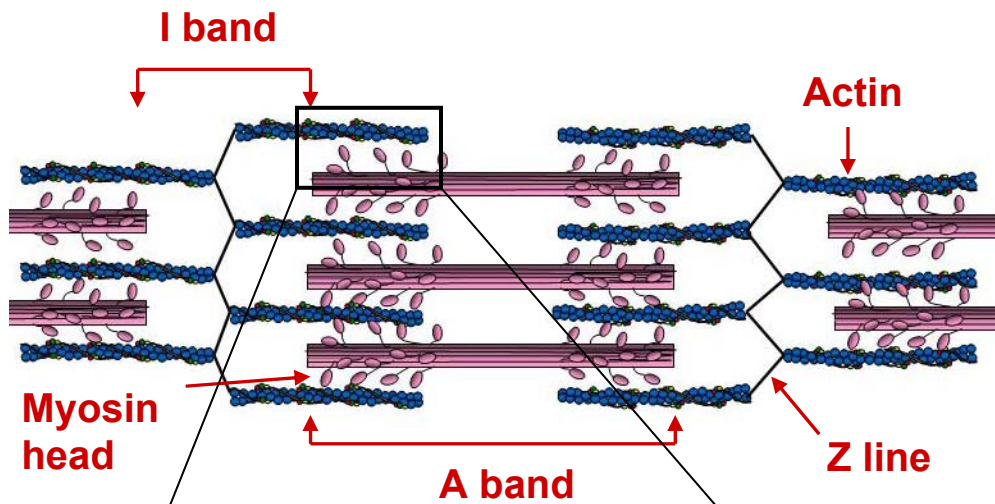
regular intervals along the thin filament is the other regulatory protein troponin. Troponin is composed of 3 polypeptide chains TnT, TnI and TnC. These polypeptides, together with tropomyosin assemble on the polymerized actin filament at a ratio of 1 Tn complex: 1 Tm dimer: 7 actins (Fig. 1B). Skeletal and cardiac muscle contraction is controlled by intracellular Ca^{2+} , where troponin is the Ca^{2+} receptive protein that plays the key role in regulating the sliding action between the two myofilaments. During muscle contraction, the filaments slide resulting in the interactions between the myosin cross-bridges with the actin thin filaments where the myosin head, binds to actin, hydrolyzes ATP and converts this chemical energy into mechanical energy for force transmission along the filaments that results in force production.

The myosin S1 fragment (subfragment-1) is the structure that forms the cross-bridges from the myosin thick filament to the actin thin filaments during muscle contraction and it is obtained by the proteolytic treatment of myosin with cysteine proteinase papain (Fig. 2A). The x-ray crystal structure of chicken skeletal S1 fragment was solved in 1993 (Rayment *et al.*, 1993a),

1.2 The Lever Arm Model and Myosin Subfragment-1

Fig. 2B illustrates subfragment 1 to be composed of both a catalytic site (where the actin binding and ATP hydrolyzing domains are) and the light chain binding domain or lever arm, an approximately 9 nm in length α -helix stabilized by two calmodulin-like light chains, the regulatory light chain (RLC) and the essential light chain (ELC). This last domain or lever arm is believed to swing while the actomyosin interface remains rigid (Cooke, 1986; Rayment *et al.*, 1993a; Holmes, 1997). In this theory, the myosin II

1A)



1B)

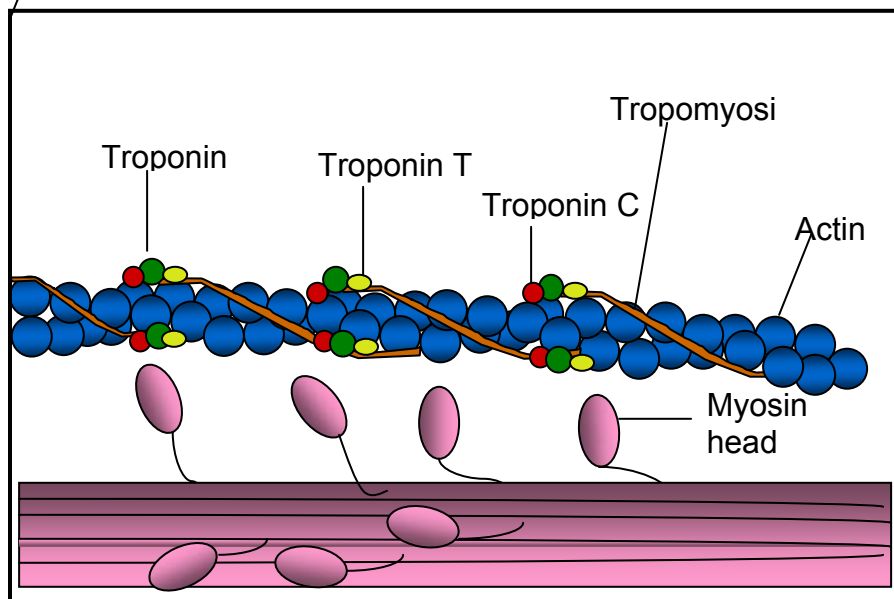


Fig 1. The sarcomere and components: A) The sarcomere is the basic unit of contraction, defined by two Z-lines. In the A band both filaments overlap, the I band is composed of only thin filament proteins. B) Inset from A: calcium binds to the troponin complex causing a conformational rearrangement of tropomyosin that makes possible the myosin-actin interaction. Actin stimulates ATPase activity in the globular myosin head that results in the production of force along the actin filaments.

heads latch onto a nearby actin thin filament and the light chain binding domain flips in a lever-like motion propelling the actin filament. The myosin head then lets go of the actin, the neck cocks back, and the head reattaches at a new point on the thin filament, starting the process again. In this manner, the lever arm of myosin is the structure that amplifies the subtle changes occurring at the actin binding and ATP hydrolyzing domains of myosin and converts them into the great molecular displacement called the “power stroke.” This power stroke is the step during the contraction cycle that pulls the actin filaments towards the center of the muscle sarcomere; its molecular mechanisms have not completely been elucidated nor have those of the effects of regulatory proteins troponin and tropomyosin in the lever arm conformations of nearby S1 heads.

To this date, “tail-wagging” or “rotating lever arm” models are being proposed based on the many structurally diverse crystallographic structural data accumulated in these past 10 years. Shorter *Dictyostelium* myosin heavy chain fragments had been crystallized in the presence of different bound nucleotides and transition state analogs (Fisher *et al.*, 1995; Smith and Rayment, 1996; Gulick *et al.*, 1997). Although these constructs were too short to carry the light chains, large-scale structural changes had been observed near the carboxy-ends of certain transition state structures where the lever arm would emerge. Up to this point, the structural data had identified two different states of myosin differing not only in the orientation of the lever arm where the most dramatic conformational changes occur but also in two more subtle changing regions of the motor domain: the 50 kDa cleft and the converter region. The first crystal structure of chicken skeletal muscle S1 without nucleotide and no actin was considered to correspond to the post-power stroke or rigor state (Rayment *et al.*, 1993a).

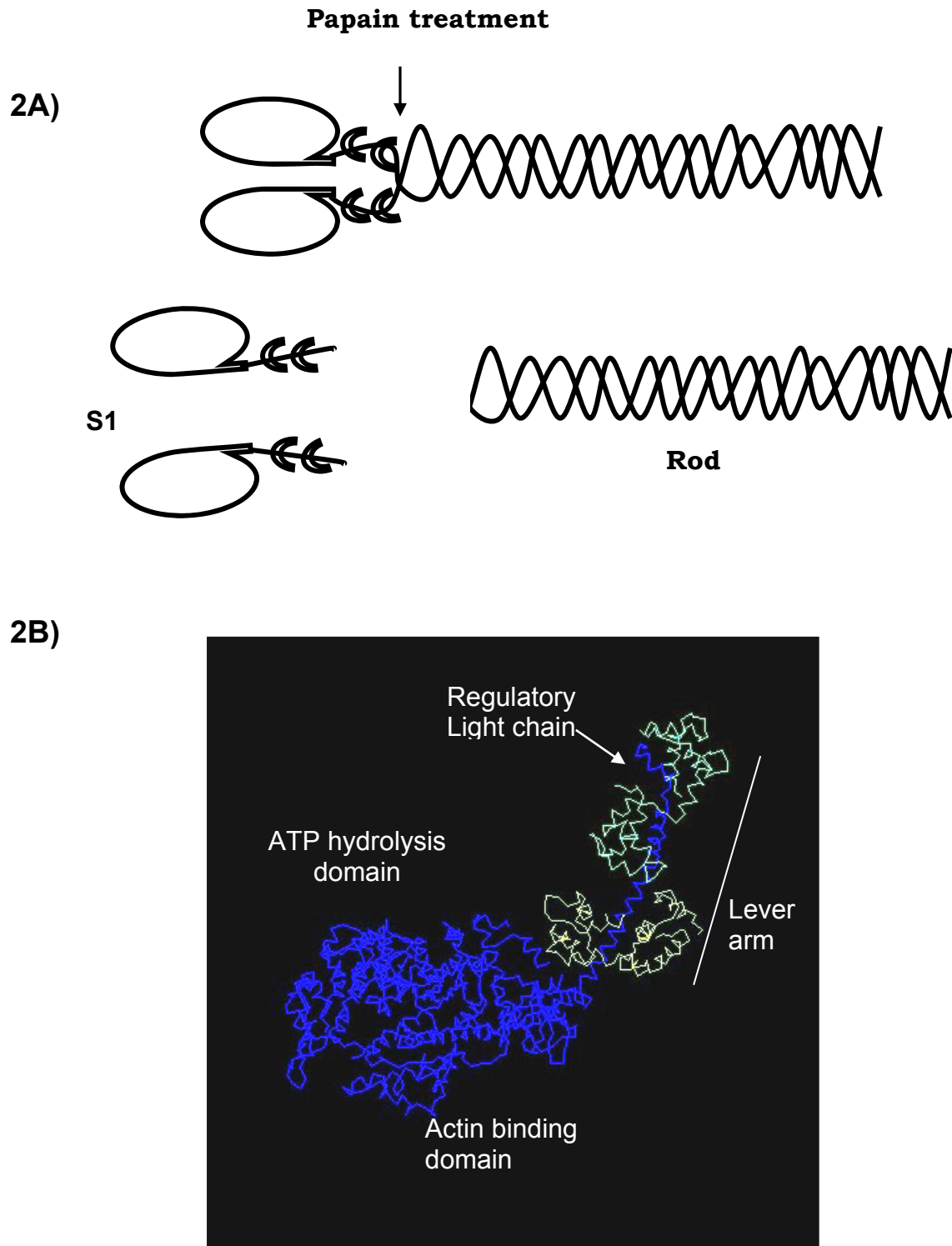


Fig 2. Myosin subfragment-1: A) Treatment of myosin with papain generates two S-1 fragments and a rod. B) X-ray crystal structure of chicken skeletal S-1 fragment (Rayment *et al.*, 1993a), the catalytic domain composed of the actin binding and ATP hydrolysis domains and the lever arm with one regulatory light chain (light green) and one essential light chain (light yellow) wrapped around.

The truncated expressed *Dictyostelium* motor domains lacking the lever arm and complexed to various nucleotide analogs were modeled in two conflicting ways; if the lever arm was present, in a “primed” transition state (lever arm in the up position) or a post-power stroke state (down position lever arm). In 1999 a scallop S1 unmodified structure complexed to MgADP with an intact lever arm revealed a third conformation of the lever arm situated almost parallel to the actin filament axis which has been interpreted as a detached ATP state occurring between the rigor and transition states (Houdusse *et al.*, 1999). The following year, the same group reported two more structural states for a total of three different conformational states of the intact scallop S1 that depend on the specific nucleotide or nucleotide analog to which it is bound: nucleotide-free motor with post-power stroke lever arm (near rigor state), transition state conformation: lever arm primed in pre-power stroke state and lastly ADP detached state. The first two conformations correspond to the span of the entire power stroke of the actomyosin cycle (Houdusse *et al.*, 2000).

1.3 Transition State Analogs of ATP Hydrolysis by Myosin

Myosin hydrolyzes ATP to produce the energy required for muscle contraction. The elucidation of the crystal structure of the S1 fragment of myosin by x-ray diffraction showed that myosin is a back door enzyme, one in which the ATP substrate binds in a site of the S1 molecule that is opposite to the binding site of the catalyst actin (Rayment *et al.*, 1993a; Fig. 2B). In the absence of ATP, the myosin S1 cross bridges bind tightly to the actin filaments. In the presence of ATP, binding to ATP causes a rapid dissociation of the actomyosin complex, therefore the crossbridges bind to either ATP or

actin but to both only transiently. Upon hydrolysis of the gamma phosphate of ATP by myosin, a stable myosin-products complex or ADP-Pi “intermediate state” is formed where the cocking of the lever arm occurs. Actin then binds to this complex and causes dissociation of the gamma phosphate ion. Kinetic observations have established that the transduction of chemical energy from the hydrolysis of ATP into mechanical force occurs during this step of product release (inorganic phosphate, Pi) rather than during the hydrolysis step. It is believed that this last step allows myosin to reverse the cocking of the lever arm while it is bound to actin causing the “power stroke” of muscle contraction. The states where myosin complexes with ATP, ADP.Pi and ADP are all intermediate states of ATP hydrolysis that have distinct spectral properties and that represent different conformations (Werber *et al*, 1972). The description of the conformations of myosin in the intermediate states is of essential importance to understand better the mechanism of myosin as a motor.

Aluminum and beryllium fluoride have been used as phosphate analogs because these small inorganic metal ions have been shown to mimic the chemical structure of a phosphate (Bigay *et al*, 1987; Chabre, 1990). A number of studies have used these nucleoside triphosphatases, including the studies showing fluoride activation of G-proteins dependent upon Al^{3+} or its substitute Be^{2+} (Sternweis and Gilman, 1982) and G-protein structural crystal studies have been done using phosphate analogs (Sprang 1997). In myosins, beryllium fluoride (BeFx) and aluminum fluoride (AlF^{4-}) complexes have been shown to substitute Pi and form a stable “locked” myosin.ADP complex where myosin is stopped from catalyzing the hydrolysis of ATP (Phan and Reisler, 1992; Weber *et al*, 1992; Maruta *et al*, 1993). The effect of these analogues on the

crystallographic structures of scallop myosins, dictyostelium myosins as well as smooth muscle myosins has also been documented. Recombinant truncated Dictyostelium S1 has been complexed with ADP.BeFx and ADP.AIF⁴⁻ (Fisher *et al*, 1995) as well as ADP-vanadate (Smith and Rayment, 1996); and the crystal structures have been solved. These studies concluded that the S1-ADP.BeFx mimics the “pre-hydrolyzed” state Myosin.ATP, whereas the S1-ADP.AIF⁴⁻ (as well as the ADP.vanadate) behaves more like a “true transition state” mimicking the Myosin.ADP.Pi intermediate state. The results from the smooth myosin S1 crystal structure however, indicate that the ADP.BeFx and ADP.AIF⁴⁻ are identical and closely resemble the Dictyostelium ADP.AIF⁴⁻ and Dictyostelium ADP.Vanadate (Dominguez *et al*, 1998). Further biochemical studies (Peyser *et al*, 1997; Phan *et al*, 1997 and Ajtai *et al*, 1999) support the conclusions from the dictyostelium results: S1.ADP.BeFx resembles Myosin.ATP whereas S1.ADP.AIF⁴⁻ (as well as S1.ADP.vanadate) resembles the Myosin.ADP.Pi intermediate state. Therefore, not only does the assigned transition state varies with the type of metal fluoride ion but it has been proposed that it varies also with the ionic strength particularly in the S1.ADP.BeFx complex (Peyser *et al*, 2001), and the presence of other contractile proteins (Phan and Reisler, 1993; Nikolaeva *et al*, 1994; Kraft *et al*, 2005).

In the present study, transition state analogs aluminum and beryllium fluoride were used in an attempt to characterize the transient weak binding states of ADP-Pi of the ATPase cycle. In the light of previous studies, assigning a particular kinetic state to any of these analogs has proven difficult due to their properties being dependent on the assay conditions and the presence of other proteins of the sarcomere. When used in

the nanocircuit in solution, both metallofluorides have exhibited no difference among themselves. However, when used in the nanocircuit in conjunction with the labeled troponin T they allowed the identification of pre-power stroke conformations and post-power stroke conformations were identified when used in conjunction with labeled tropomyosin. The goal of the spectroscopic nanocircuit is to not only identify different conformations of the lever arm by averaging the signals from a large number of molecules but to exploit the signal of the last acceptor of the nanocircuit relay to identify the most critical conformations to a given transition kinetic step using the analogs.

1.4 Objectives

The different possible orientations of the light chain binding domain mapped by x-ray crystallographic methods need to be corroborated by studies done in solution and in the presence of the other regulatory components of muscle contraction to establish their dynamic interaction. Fluorescence spectroscopy is a technique that can resolve distances of subnanometer length and together with crystallography can provide additional detailed information for the understanding of the molecular mechanisms of contraction and motility. As opposed to x-ray crystallography, fluorescence spectroscopic methods allow the measurement of conformational changes observed in dynamic form and closer to physiological conditions. The different kinetic states of myosin reflect different stages in the ATPase cycle and great effort has been put into correlating these stages to the available structural data. Additionally, spectroscopic data, by virtue of being collected in solution, has shown that it is a distribution of myosin structures that are present at any given time so that a particular kinetic state may

correspond to several structures. This novel fluorescent nanocircuit assay was developed with the objective of studying the molecular dynamic interaction of the proteins involved in skeletal muscle contraction in solution using fluorescence resonance energy transfer (FRET) and luminescent lanthanides as energy transfer donors. In solution, the nanocircuit makes possible the measurement of the kinetic states of myosin through the averaging of a number of molecules, while the three relay system ensures that only the molecules bound to the filament and bound closest to any of the two labels in the thin filament: either Cy7-Troponin T or Cy7-Tropomyosin α , are averaged in the readings. The purpose is to identify more clearly which conformations are more critical to the weak binding state by looking at the changes in position of the RLC relative to the nucleotide binding site of molecules bound proximate to two different parameter proteins in the thin filament in the presence and absence of ADP and nucleotide analogs. Furthermore, the nanocircuit provides a way to assess the location of regulatory protein, troponin T, on the thin filament relative to myosin during the actomyosin interaction in the presence and absence of calcium. The present work is first in its kind to label in solution three different sites of the actomyosin cycle as a relay of energy successfully.

Measurement of distances to establish lever arm movement using energy transfer between two sites: the light chain and catalytic domain before and after the power stroke have been done in the past. (Shi *et al.*, 2000; Xu and Root, 1998 and 2000, Smoczynski and Kasprzak, 1997). Additionally, the determination of the crystal structures of the troponin complex (Takeda *et al.* 2003. and Vinogradova *et al.* 2005) has further advanced the knowledge of the regulation of muscle contraction at the

molecular level but still much of the interactions of all the actomyosin components remain to be elucidated.

This novel nanocircuit assay, allows measurements in three different sites as a relay of energy transfer that involve myosin as well as the muscle regulatory proteins of the thin filament. Being the first time that a third parameter is used to study conformations of the lever arm, this nanocircuit is a unique assay. For it not to break, the terbium-labeled RLC in the lever arm, the Cy5-ADP in the nucleotide binding site and a proximate troponin T or tropomyosin α must be no farther than their R_0 Forster distance for energy transfer to occur. In that case, no time-resolved fluorescence signal would be observed from Cy7, the last site of the relay.

The hypothesis tested in this study is the hindrance posed by the periodically situated troponin complexes to myosins that when binding adjacent to the Tn complex situated every 7 actin monomers along a thin filament, are unable to complete their power stroke. Furthermore, this study tests the lack of hindrance measured in the lever arm conformations of myosins bound in between the Tn complexes.

CHAPTER 2

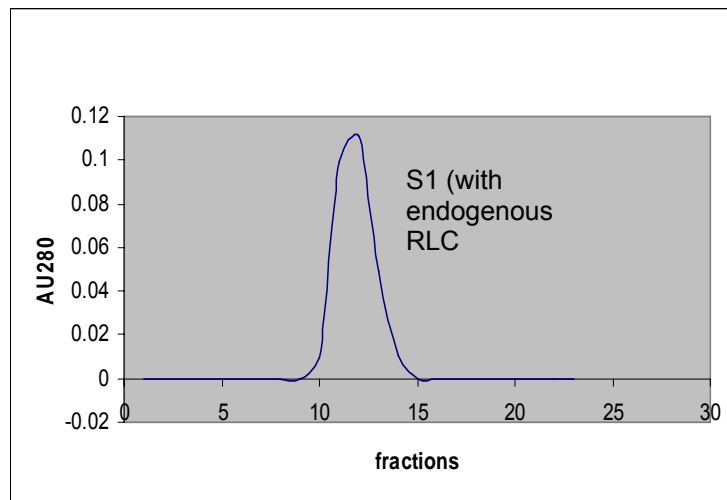
EXPERIMENTAL MATERIALS AND METHODS

2.1 Preparation of Myosin Subfragment-1 by Papain Treatment and Endogenous RLC Heat Extraction

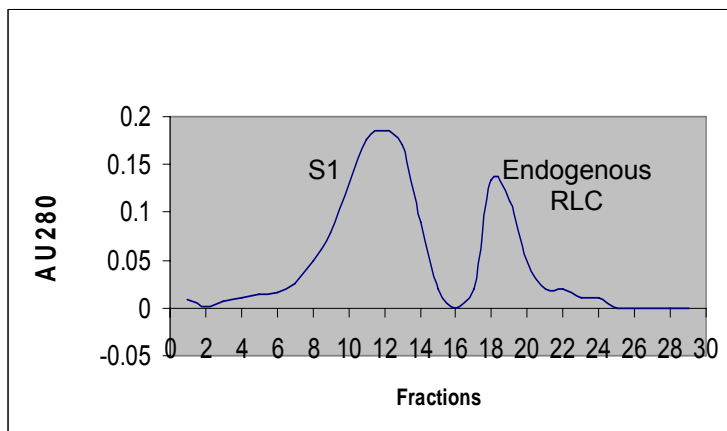
Myosin subfragment 1 (S-1) was prepared by papain digestion of rabbit skeletal myosin. Myosin (stored flash-frozen) in 0.5 M KCL, 10mM imidazole, pH 7.0 was centrifuged at 100,000 x g (47,000 rpm) in a TLA 100.3 rotor (Beckman Optima™ TL-100 ultracentrifuge) for 1 hour at 4°C to remove aggregates. The cleared supernatant was dialyzed against 1 L of 0.1 M KCl, 10mM imidazole, pH 7.0 for 15 hours (overnight) at 10°C, lowering the salt concentration causes the myosins to form filaments. The next day, MgCl₂ was added to a final concentration of 2 mM prior to digestion. Fresh papain was added to a final concentration of 0.2 mg/mL to the protein solution and incubation was done for 7 minutes at 25°C or room temperature in a shaker. The proteolytic reaction was stopped by the addition of 50 ul of E-64 (from SIGMA) per ml of myosin solution. The products were dialyzed 15 hours (overnight) against 1 L of 0.04 M KCl, 10 mM imidazole, pH 7.0. The next day ultracentrifugation at 100,000 x g (47,000 rpm in a TLA 100.3 rotor) for 1 hour at 4°C yields S1 in the supernatant (Fig. 3A). The S1 preparation (containing the endogenous Regulatory Light Chain (RLC)) was run through a first Toyopearl® 55-F gel filtration column to buffer exchange the protein to 50 mM Kpr, 20 mM EDTA, 10 mM Kpi, 0.5 mM DTT, pH 7.0 (Fig. 3A). The eluted S1 in K propionate buffer was heated at 30°C for 15 minutes to extract the endogenous RLC. Separation of the stripped RLC was accomplished by a second Toyopearl® 55-F gel filtration step after heat removal (Fig. 3B). Fig. 3C shows the 12% SDS-PAGE of S1 devoid of RLC with a molecular weight of about 95 kDa as compared to broad-range

prestained SDS-PAGE standards from Bio-Rad.

3A)



3B)



3C)

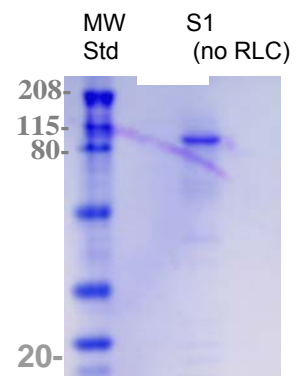
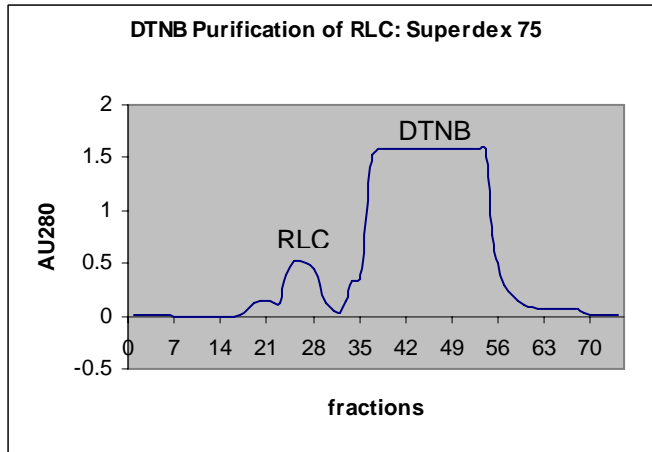


Fig 3. Papain digested subfragment-1 and RLC heat removal. Gel filtration chromatography after papain digestion (3A). Gel filtration after heat removal of regulatory light chain (3B). SDS-PAGE of S1 devoid of RLC at expected MW of 90 kDa (3C).

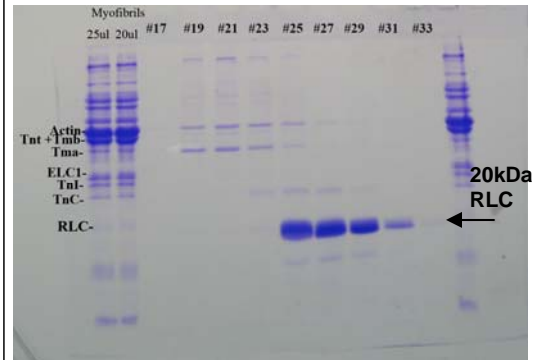
2.2 DTNB Purification and Terbium Chelate Conjugation of RLC

RLC was dissociated from rabbit skeletal muscle myosin with DTNB (Wagner, 1982) and purified by β -mercaptoethanol reduction followed by Superdex™-75 gel

4A)



4B)



4C)

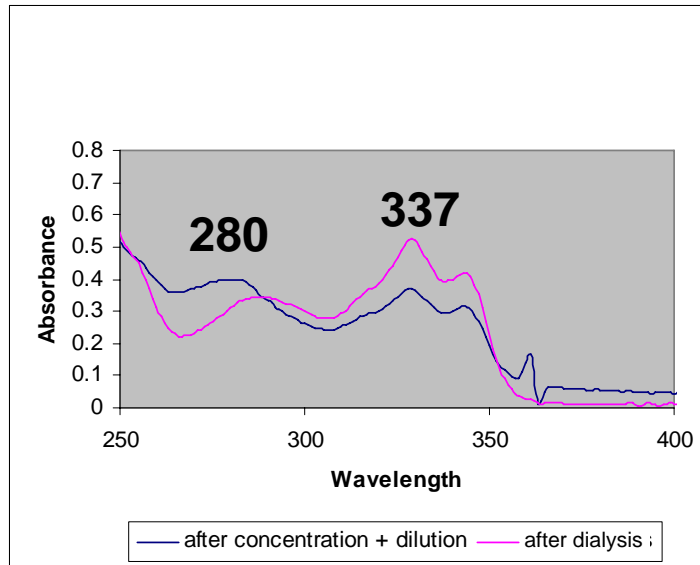


Fig. 4. RLC purification and labeling. Dissociation of RLC achieved by treatment of myosin with sulfhydryl reactant DTNB followed by BME reduction and separation by Superdex-75 gel filtration chromatography (4A). 15% SDS-PAGE gel indicating the separation of high purity RLC (fracs 25-31) from higher molecular weight myosin heavy chain and thin filament regulatory proteins (fracs 17-22) and from excess DTNB (fracs 34-55)(4B). Absorption spectra of removal of excess CS124-DTPA terbium chelate from labeled RLC after desalting and dialysis (4C).

filtration chromatography to remove excess Ellman's reagent (Fig. 4A). RLC of high purity was obtained as shown by a 15% SDS-PAGE of the eluting fractions 25-31 from the FPLC and removal of excess DTNB reagent in fractions 34-58 (Fig. 4B).

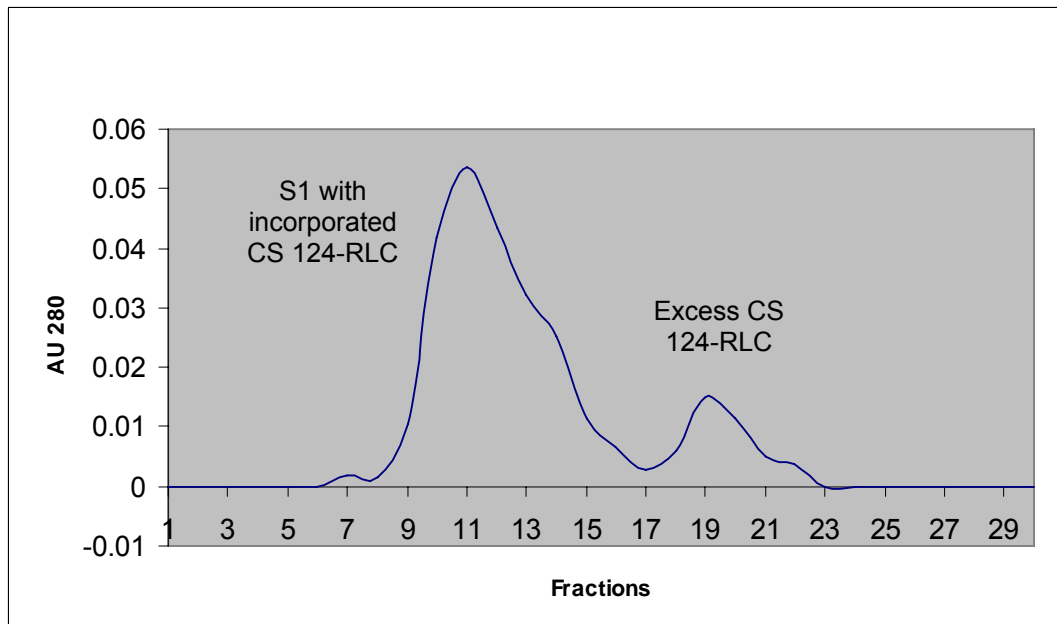
The purified rabbit skeletal RLC was labeled with a 1,500 x molar excess of an equimolar mixture of carbostyryl-124 and DTPA in DMSO to conjugate terbium with DTPA/ CS124. DTPA is a dianhydride reagent that attaches to carbostyryl via one anhydride, the other one interacts with the amine groups of lysine residues of RLC. The great excess of free reagents were dialyzed over a weekend and subjected to several rounds of buffer exchange by concentration and dilution using a Millipore Centricon® centrifugal filter device with a membrane of a molecular weight cut off of 5,000; 4 times smaller than the RLC protein's molecular weight (Fig. 4C).

2.3 CS 124-Tb-RLC Exchange to S1 and Labeling Ratio by Terbium Titration

Cs-124 labeled RLC was added at molar excess to S1 to be exchanged back with overnight dialysis in 1 mM MgCl_2 , 0.1 M KCl and 10 mM imidazole, pH 7 overnight. The next day, excess free labeled RLC was separated by Superdex™ 75 gel filtration (Fig 5A) and protein was concentrated using Centricon® concentrators to 2 μM (about 0.25 mg/ml) as read on a HP UV-Vis spectrophotometer (extinction coefficient for S1 is $0.75 \text{ ml mg}^{-1} \text{cm}^{-1}$)

Terbium titration was carried on an SLM-Aminco Bowman II luminescence spectrometer (Spectronic Instruments, Rochester, NY) with dual xenon arc and flashlamp light sources. Titration was carried by incubating the CS 124-RLC-S1 with increasing amounts of terbium chloride solution. Excitation was set at 337 nm with emission collected at 547, the intensity of emission was plotted against the concentration of terbium chloride, indicating a 100% labeling ratio (Fig. 5B)

5A)



5B)

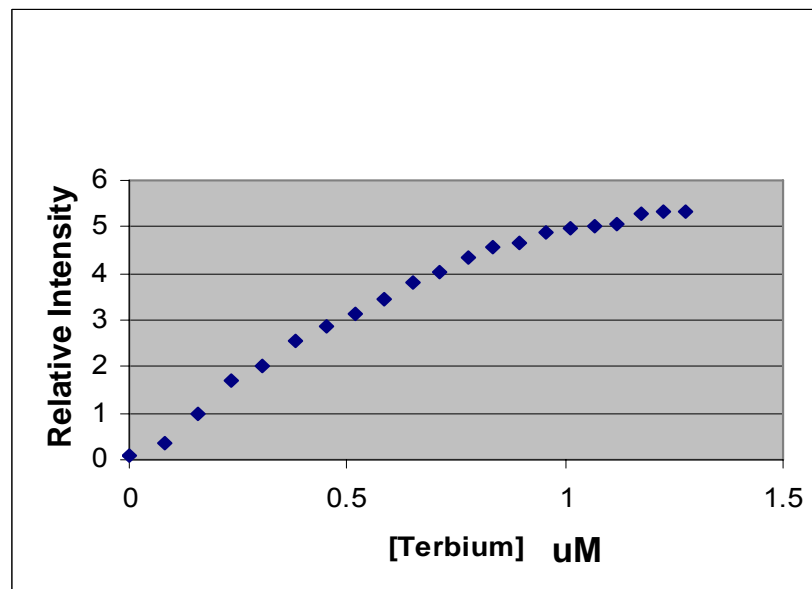


Fig 5. CS 124-Tb-RLC exchange into S1 and labeling efficiency. FPLC Superdex-75 separation of residual CS 124-Tb-RLC after exchange to S1 previously devoided of endogenous regulatory light chain (5A). Labeling ratio of 1 to 1 or 100 % labeling efficiency calculated by terbium titration of CS 124-Tb-RLC-S1 as estimated by following the luminescence enhancement and saturation upon titration of 0.9 μ M S1 with 0.9 μ M terbium chloride solution (5B).

2.4 Tropomyosin- α Purification and Cy7 Labeling

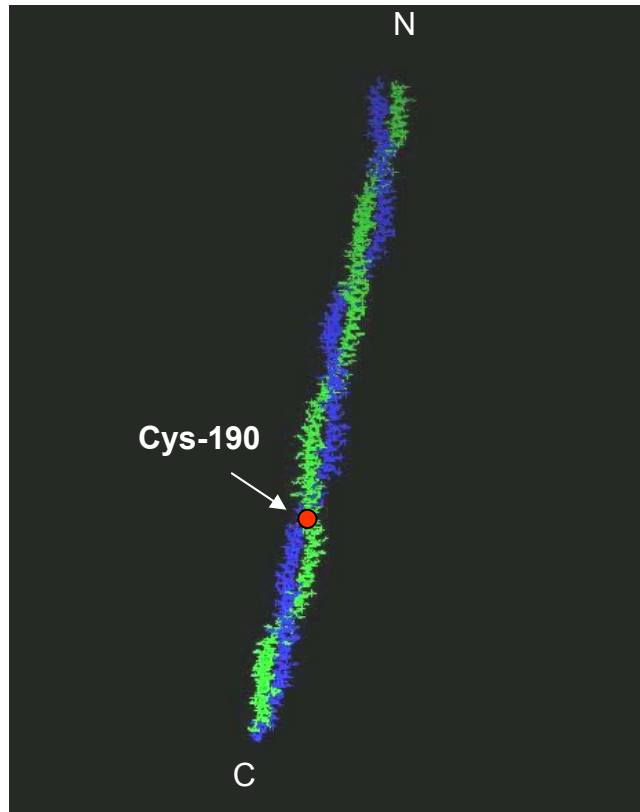
Tropomyosin was extracted from acetone powder from rabbit skeletal back

muscle mince in 1.0 M KCl, 0.5 mM DTT at pH 7 according to a modified protocol of Bailey and further purified as α,α - and α,β -tropomyosin by hydroxyapatite chromatography as the method described by Cummins and Perry (Colowick, 1982). The proteins were eluted by a linear gradient of 1-200 mM phosphate buffer to separate the two subfractions: α (higher electrophoretic mobility) and β subunits (Fig. 6). The α subunit contains a single cysteine residue, whereas the β subunit has two cysteine residues per 33 kDa. The single cysteine containing Tm- α was picked for labeling. Fractions containing only α,α -tropomyosin were pooled to a final concentration of 4 mg/ml and were denatured by dialysis in 6 M urea and 10 mM imidazole pH 7. Labeling was carried at denaturing conditions of 6 M urea with Cy7-maleimide with the purpose of labeling the single Cys 190 residue in the rabbit Tm- α . Cys 190 is involved in disulphide crosslinking of the polypeptide chains of a dimer and it is highly conserved in the α tropomyosins in human, pig, rat and rabbit (Perry, 2001). The labeled protein was flash frozen for storage until needed.

The troponin subunits were purified after the tropomyosin extraction from rabbit skeletal muscle in denaturing conditions 6 M urea with FPLC chromatography in a DEAE-Sephadex A-50 column as described in Colowick (Colowick, 1982), with an additional chromatography step with Sephadex G50/75 for the removal of lower molecular weight contaminants in the troponin I subunit isolation.

The Cy7 labeled troponin T subunit used is a naturally occurring isoform from skeletal avian breast muscle that has calcium binding properties and a single cysteine used for the attachment of different fluorescent probes (Jin and Root, 2000; Zhang *et al.*, 2004)

6A)



6B



Fig 6. Tropomyosin α . Tm α molecule 7Å resolution crystal structure from porcine ventricles crystallized by Whitby and Philips in 2000, showing Cys 190 highly conserved residue in pig, human, rat and rabbit (6A). 15% SDS-PAGE of hydroxyapatite separation of tropomyosins α (higher electrophoretic mobility) and β from rabbit skeletal muscle (6B)

2.5 Nanocircuit Assay in Solution

The acto-S1-Tropomyosin-Troponin complex experiments were performed in 0.1 M KCl, 2 mM MgCl_2 , and 10 mM imidazole, pH 7.0. The concentrations in the assay of labeled S1 were 0.5-0.8 μM , while the molar ratios of S1 to actin assayed were 1:1 and 1:7 in order to analyze two conditions: saturating or 1 S1 per 1 actin molar ratio and at 1 S1 per 7 actin molar ratio. Since TnT repeats at every 7 actin monomers, the idea is to measure if crowding of S1 heads affects lever arm conformations in the saturated versus the non saturated conditions. No significant effect of actin saturation with myosin S1 was clearly observed, therefore for detection efficiency purposes, saturating conditions were used. Actin was reconstituted by dialysis in assay buffer and assembled with 1/7 ratio of renatured tropomyosin, troponin I, C, and Cy7 troponinT. The complex is added to the system (case I, Fig. 7). The same ratios apply to the thin filament reconstitution involving the Cy7 label at tropomyosin α (case II, Fig. 7). Other conditions are measured with no nucleotide, with CY5-ADP at final equimolar amounts to S1, with transition analogs beryllium and aluminum fluoride (at 0.1 mM final concentration) and + and – calcium removed by the addition of EGTA at also 0.1 mM final concentration of CaCl_2 .

All contractile protein components were mixed in a 100 μl total volume reaction in an eppendorf UVette® without CY5-ATP for a “donor” only measurement of emission and decays at 540 nm, 690 nm and 780 nm in the appropriate buffer. First acceptor CY5-ADP labeling the nucleotide binding pocket was added as CY5-ATP for the nanocircuit to occur and appropriate signals were read after a 5 minute incubation (to allow ATP hydrolysis) at 540 nm, 690 nm and 780 nm as well.

Papain, DTPA, beryllium, aluminum chloride, sodium fluoride, and terbium chloride hexahydrate were obtained from Sigma Aldrich. Cy5 and Cy7 from Amersham-Pharmacia Biotech.

2.6 Nanocircuit LRET Measurements

An SLM-Aminco Bowman II luminescence spectrometer (Spectronic Instruments, Rochester, NY) with dual xenon arc and flashlamp light sources was used to record luminescence spectra. Delayed lifetime measurements were collected after 200 μ s following the excitation pulse of the flashlamp to the laser at 337. Delayed emission spectra were accumulated after a 200 μ s delay after flash with a gate width of 4.5 ms. Luminescent decay curves were accumulated at a resolution of 200 μ s and averaged for 200 repetitions to increase the signal-to-noise ratio. The donor of the resonance energy transfer relay was terbium in the RLC. The terbium signal was enhanced by the chromophore carbostyryl 124, which transfers energy to terbium by excitation at 337 nm with a nitrogen laser with a bandpass of 16 nm. The sensitized emission of the fluorescent acceptors were recorded at 547 nm (for terbium) with a bandpass of 4 nm; at 690 (for Cy5-ADP) with a bandpass of 4 nm; and at 780 nm (for Cy7 TnT) at high voltage and a bandpass of 8 nm. Sensitized emissions are only detected if the resonance energy transfer occurs, because the delay allowed after the pulsed excitation signal causes background fluorescence such as Raman and light scattering to decay to negligible levels before the data is collected.

2.7 Data Analysis: Single and Double Exponential Fitting of Decay Curves

Emission scans with donor only and in the presence of acceptors were subtracted of a baseline, and instrument correction was performed to compensate for the lack of sensitivity of the photomultiplier after wavelength 600 nm. Final curves were smoothed to 15 points and exported to excel for plotting as shown in Fig. 8. The nanocircuit is broken if any of the three components is farther apart than their R_0 distance for energy transfer to occur, so the decay of signal from the terminal acceptor reports on the conformation of myosin S1 bound near troponin (or tropomyosin) while the decays of previous fluors of the circuit report on the average conformations of all S1 regardless of their position (Fig. 9).

The lifetimes of the decay curves were calculated by MacCurveFit Software (version 1.3.3 by Kevin Raner). Lifetimes at 547 nm were fitted single and double exponentially to account for the molecules that are bound to actin and the ones unbound as illustrated in Fig. 9. The efficiency of energy transfer (E) and distance (R) between donor and acceptors were determined by comparing lifetime measurements of the donor without the acceptor present and the sensitized emission of the acceptor in the presence of the donor per equations 1, 2, and 3 (section 1.6).

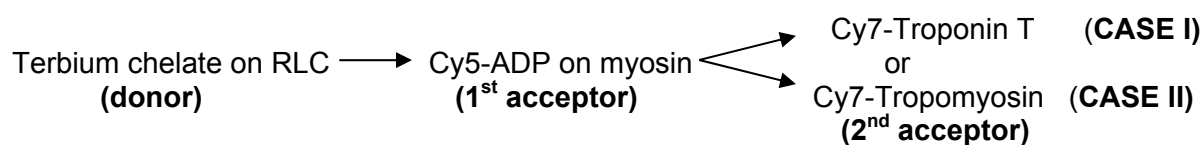
CHAPTER 3

EXPERIMENTAL DESIGN

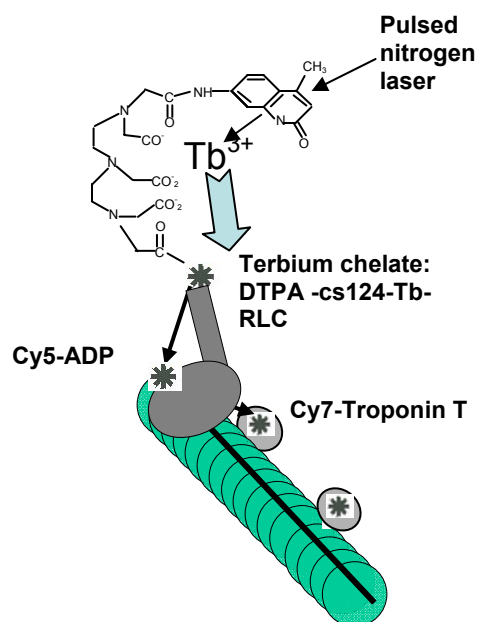
3.1 Nanocircuit Components

A relay of three different fluorescence resonance energy transfer sites (depicted by the asterisks in Fig. 7), label three different components in the contractile mechanism using LRET (lanthanide-based resonance energy transfer. LRET is FRET that employs luminescent lanthanides as energy transfer donors. Terbium, is a rare earth metal element that belongs to the lanthanides with a very long lifetime of milliseconds, about one million times longer than the two different Cy dyes acting as acceptors in this system. Prepared as a chelate, Tb-DTPA-cs124, has a slow decay that gives greater accuracy than conventional FRET in measuring distances due to the donor emission being unpolarized.

The nanocircuit is assembled first by attaching to the rabbit skeletal myosin regulatory light chain a terbium chelate. The terbium chelate as a donor allows the determination of efficiency of energy transfer by measuring the sensitized emission lifetime that is a consequence of energy transfer. The small size terbium emits light isotropically with low background and less complications of orientation factor artifacts that conventional organic fluorophores have. Carbostyryl-124 is an organic chromophore that absorbs light at 337 nm of wavelength. Cs-124 participates with DTPA in the chelation of terbium. It is used as an excitation antenna that upon excitation with a pulsed nitrogen laser at 337 nm, transfers energy to the lanthanide terbium overcoming the weak absorption cross-section that this lanthanide alone inherently possesses. The excited lanthanide then transfers energy to the nucleotide



CASE I



CASE II

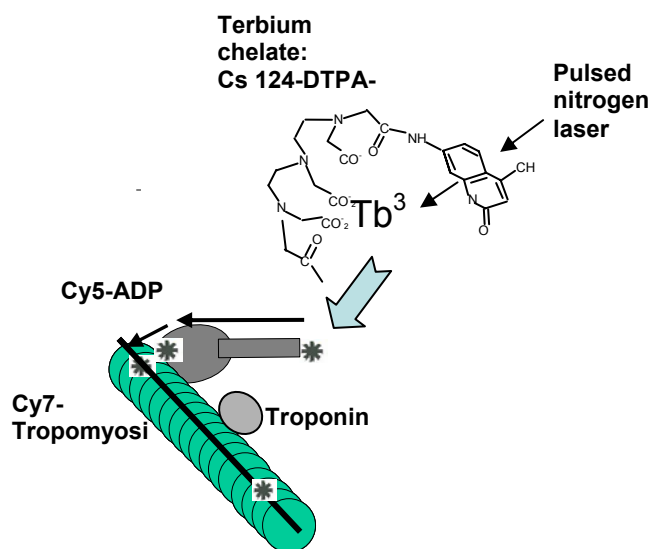


Fig 7. Components of the nanocircuit relay. Donor, 1st acceptor and two possibilities for a 2nd acceptor. Excitation of the CS-124 antenna with a pulsed laser excites the terbium chelate on the lever arm which transfers energy to its acceptor, Cy5-ADP on labeling the nucleotide binding site of myosin, which in turn relays the energy to any of the two last acceptor on the thin filament: Cy7-troponin (case I) or Cy7-tropomyosin α (case II)

binding site which is the second relay site and first acceptor of energy labeled by Cy5-ADP. This second site in turn transfers energy to the third and last relay site: the Cy7 attached to a unique single cysteine in the alternative splicing isoform of Troponin T or to Cys 190 in the Tropomyosin α subunit in the thin filament. Both cases are illustrated with asterisks in Fig. 7.

3.2 Theory of Luminescence Resonance Energy Transfer (LRET)

The efficiency (E) of energy transfer between the donor lanthanide chelate in the RLC and the acceptor 1 (Cy5-ADP) or acceptor 2 (Cy7-TnT) was determined by comparing the lifetime measurements of the donor without the acceptor present and the “sensitized” emission of the acceptor in the presence of the donor by using the equation:

$$E = 1 - \tau_{da}/\tau_d \quad (\text{Eq. 1})$$

Where τ_{da} is the apparent lifetime of the sensitized emission of the acceptor in the presence of the donor since the delayed acceptor fluorescence should be due only to the energy transfer from the donor and τ_d is the lifetime of the donor alone.

Furthermore, the efficiency of LRET (E) for the distance (R_i) between donor and acceptor was calculated from the equation:

$$E = \sum_i (R_o^6/R_i^6) / (1 + \sum_i (R_o^6/R_i^6)) \quad (\text{Eq. 2})$$

Where R_i is the actual separation distance between donor-acceptor pair and R_o is the critical transfer distance that corresponds to a distance of 50% energy transfer efficiency and calculated as follows:

$$R_0 = 8.79 \times 10^{-11} J \kappa^2 \eta^{-4} \phi_D)^{1/6} \text{ nm} \quad (\text{Eq. 3})$$

Where J is the calculated overlap integrals for the acceptor with the donor; κ^2 is the dynamic average value of the orientation factor, $2/3$; the isotropic emission of terbium will limit the orientation factor uncertainty of at the most, 10% (Selvin and Hearst, 1994)

From equation 2, efficiency of energy transfer “E”, it is observed that FRET diminishes as the sixth power of the distance between the donor and the acceptor; therefore, no FRET occurs for distances greater than $2 R_0$. Since R_0 is on the order of 10 to 70 Angstroms, by performing FRET measurements it is possible to distinguish proteins that are merely nearby in the same vicinity from those proteins that are interacting with each other. R_0 depends on the relative orientation and spectral properties of the two dyes and the donor quantum yield. The calculated R_0 for the terbium-Cy5 pair is 5.1 nm.

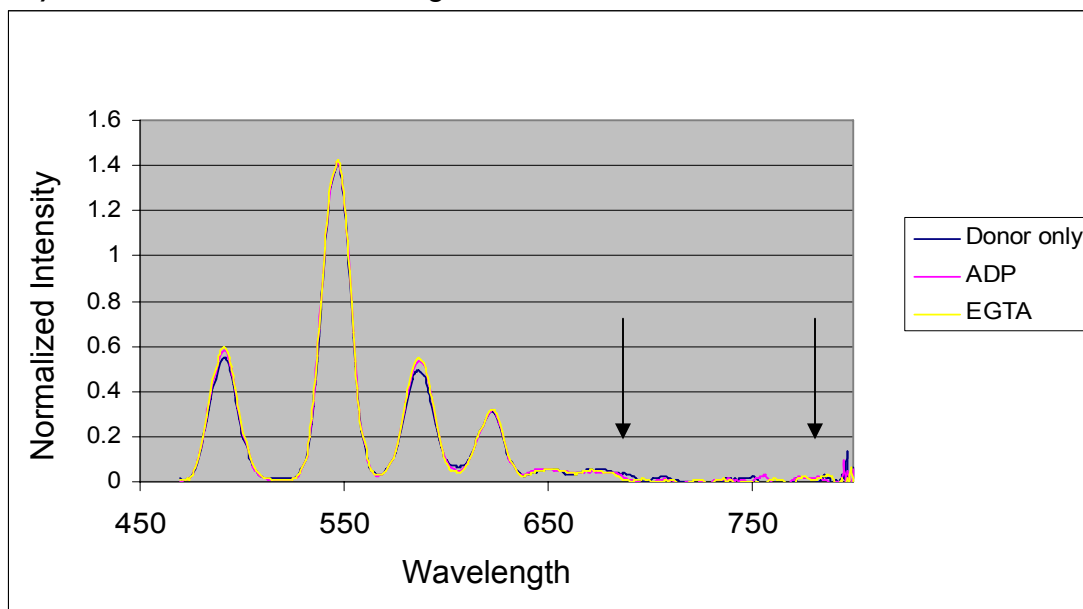
CHAPTER 4

RESULTS

4.1 FRET Strategy: No Cross Contamination Between Donor and Last Acceptor

In this study, the RET (resonance energy transfer) strategy was to pick three appropriate labeling probes: a terbium chelate as the donor and two different organic dyes as acceptors of well separated emission spectra. The energy transfer circuit breaks if any of the three components is farther than R_0 critical transfer distance. As a donor, the terbium chelate provides great advantages such as a millisecond lifetime following the excitation of the nitrogen excitation pulse, a high quantum yield and lack of polarization. In this manner, the emission that is recorded from the acceptors due to energy transfer (the sensitized emission) gets measured with no background contamination and the determination of distances is highly accurate due to the no polarity characteristic of the terbium chelate. Fig. 8A shows that after adding ADP to the assay with donor and last acceptor, no conformational changes are reported at 780 nm unless the middle acceptor Cy5-ADP is added as shown in Fig. 8B. Additionally Fig. 8B illustrates that when the donor and last acceptor are in the assay without Cy5-ADP, no energy transfer due to cross-contamination is observed between the RLC (donor) and the last acceptor tropomyosin α until Cy5-ADP is added when time-resolved fluorescent emission changes are observed at both 690 and 780. Consequently, Cy7 signal at 780 nm only reports RET of myosins bound to actin and adjacent to labeled tropomyosin.

8A) Broken nanocircuit using ADP:



8B) Nanocircuit emission using Cy5-ADP:

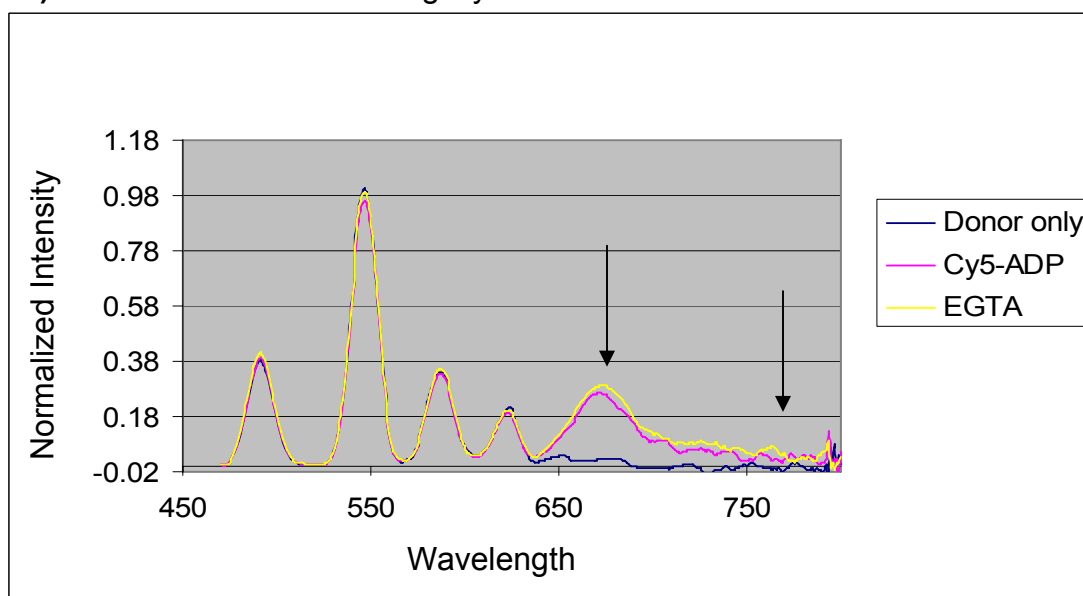


Fig 8. Nanocircuit: no cross contamination between donor and last acceptor. Nanocircuit with second acceptor Cy7-tropomyosin α . In the presence of unlabeled ADP, no energy transfer is observed between the RLC (donor) and the last acceptor tropomyosin- α showing no cross-contamination between these two labeling sites representing a “broken” energy transfer circuit (8A). Donor only and nanocircuit occurring after the addition of Cy5-ADP (first acceptor), causing time-resolved fluorescent emission changes at both 690 and 780. Consequently, Cy7 signal at 780 nm only reports RET of myosins bound to actin and adjacent to labeled tropomyosin.

Fig. 9 shows the complete emission scans of the assay performed with second acceptor Cy7-TnT at different conditions: S1 molecules bound to Cy5-ADP, or CY5-ADP.AIF4 and in the presence of calcium chloride and absence of calcium by chelation with EGTA.

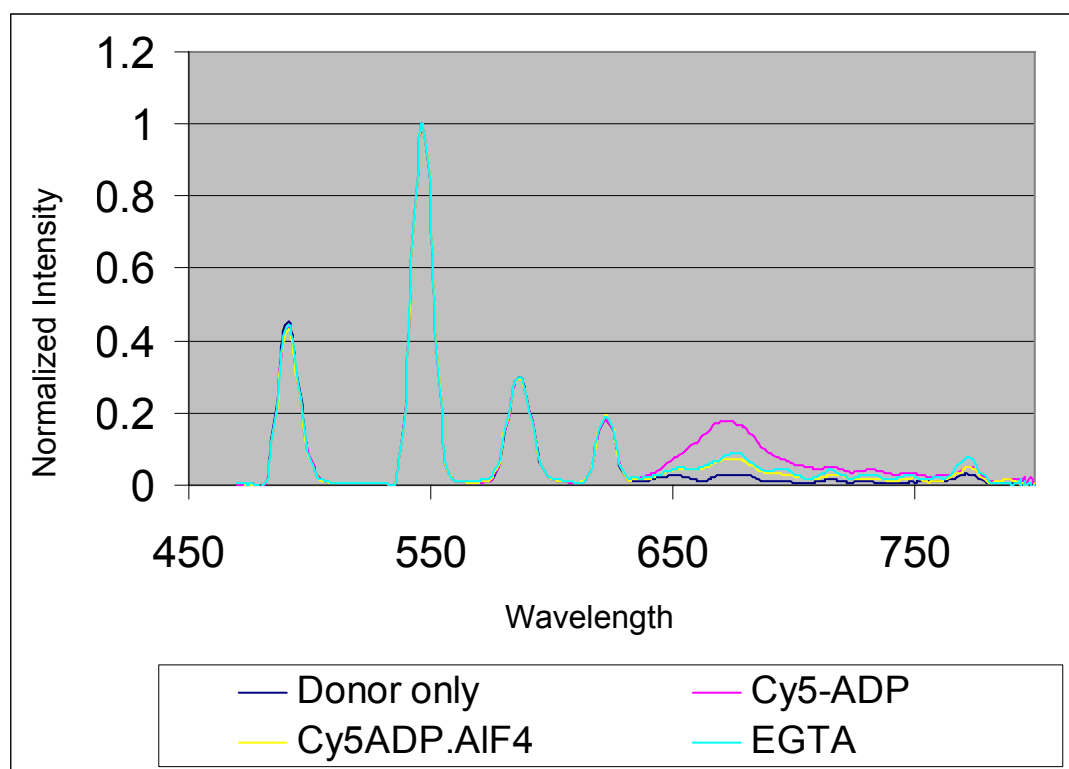


Fig. 9: Emission spectra of complete nanocircuit assay with troponin T label. The complete emission spectra of a nanocircuit assay with Cy7-TnT as second acceptor. Donor is Tb chelate-RLC (donor only in blue), first acceptor Cy5-ADP (magenta) or Cy5-ADP.AIF4 (yellow) and second acceptor Cy7-TnT. Assay conditions were performed in the presence of Ca^{2+} ; until removal by the addition of EGTA (yellow)

4.2 Nanocircuit LRET Distances Compared to X-ray Diffraction and Other FRET Measurements of the Myosin Lever Arm to the Nucleotide Binding Site

Table 1 compares two distances a short (pre-power stroke) and a longer one (post-power stroke) calculated from the nanocircuit measurements and shown in bold. When measured from the sensitized emission of Cy5-ADP to regulated actin in the

presence of calcium, the distance between the N-terminus of the RLC and the nucleotide site was 6.6 ± 0.6 nm, and when measured from the sensitized emission of the donor in the presence of Cy5-ADP with regulated actin and calcium using the third probe at tropomyosin, a similar distance of 6.50 ± 0.01 nm were obtained. The same measurement done when troponin T is the third probe yields a similar distance of 6.4 ± 0.4 nm. These distances correspond to post-power stroke states of the lever arm and have a great resemblance to measurements of 6.6 nm and 6.9 nm in the absence of actin and presence of unregulated actin respectively as previously reported with different donor/acceptor pairs labeling the same sites and using FRET in solution (Xu and Root, 1998). Additionally, in the chicken skeletal muscle myosin crystallographic structure in the absence of nucleotide, a distance of 6.6 nm, was reported between TRP 131 at the nucleotide site and GLY 21 on the essential light chain which is the aminoacid in the crystal structure that is closest to the location of the label in the N-terminus of the RLC (Root, 2002b).

Distances corresponding to the pre-power stroke state of the lever arm, were widely observed using the LRET nanocircuit mostly through the sensitized emission from the troponin T label with Cy7 and observed a lever arm at a very definite pre-power stroke state. Values of a shorter distance such as 5.6 ± 0.25 nm in the presence of ADP and calcium as well as 5.5 ± 0.3 nm in the presence of calcium and transition state analogs $\text{AlF}_4\text{-ADP}$, or 5.6 ± 0.6 with calcium and BeFx-ADP were repeatedly observed. All these values fit close with a value of 5.1 nm reported between equivalent residues in the crystal structure of chicken smooth muscle myosin complexed with $\text{AlF}_4\text{-ADP}$ (Root 2002b). The typical distance differences of about 1-1.5 nm observed in energy transfer

Table 1: Fluorescent nanocircuit analysis of lever arm position: comparison of conformations of myosins bound to thin filaments proximate to TnT versus tropomyosin. Compares two distances a short (pre-power stroke) and a longer one (post-power stroke) calculated from the nanocircuit measurements in bold between S1 myosins bound proximate to the troponin complex or in between troponin complexes along tropomyosin.

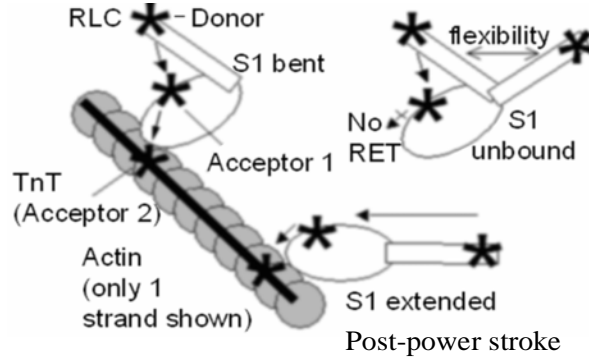
| Sample | Nucleotide | Wave-length (nm) | Exponentials in fit | 2 nd accept: TroponinT E R(nm) | | 2 nd accept: Tropomyosin E R(nm) | |
|--------------------------|----------------------|------------------|-----------------------|--|----------------|--|------------------|
| Acto-S1+Ca ²⁺ | ADP | 547 | Single | 0.22±0.07 | 6.4±0.4 | 0.19±0.00 | 6.50±0.01 |
| Acto-S1+Ca ²⁺ | ADP | 547 | Multiple ^a | 0.46±0.14 | 5.4±0.5 | N/A | N/A |
| Acto-S1+Ca ²⁺ | ADP | 690 | Single | 0.19±0.1 | 6.6±0.6 | --- | --- |
| Acto-S1+Ca ²⁺ | ADP | 780 | Single | 0.40±0.05 | 5.6±0.2 | 0.27±0.03 | 6.02±0.17 |
| Acto-S1+Ca ²⁺ | ADP-BEFx | 547 | Single | 0.16±0.11 | 6.8±0.7 | 0.21±0.00 | 6.37±0.02 |
| Acto-S1+Ca ²⁺ | ADP-BEFx | 547 | Multiple ^a | 0.61±0.2 | 4.8±0.6 | N/A | N/A |
| Acto-S1+Ca ²⁺ | ADP-AIF ₄ | 547 | Single | 0.13±0.05 | 7.1±0.4 | 0.15±0.02 | 6.79±0.15 |
| Acto-S1+Ca ²⁺ | ADP-AIF ₄ | 547 | Multiple ^a | 0.73±0.2 | 4.2±0.6 | N/A | N/A |
| Acto-S1+Ca ²⁺ | ADP-BEFx | 780 | Single | 0.38±0.17 | 5.6±0.6 | 0.25±0.04 | 6.13±0.19 |
| Acto-S1+Ca ²⁺ | ADP-AIF ₄ | 780 | Single | 0.41±0.09 | 5.5±0.3 | 0.23±0.06 | 6.24±0.34 |
| Acto-S1+EGTA | ADP-BEFx | 547 | Single | 0.12±0.07 | 7.1±0.6 | 0.24±0.01 | 6.20±0.04 |
| Acto-S1+EGTA | ADP-BEFx | 547 | Multiple ^a | 0.38±0.1 | 5.7±0.1 | N/A | N/A |
| Acto-S1+EGTA | ADP-AIF ₄ | 547 | Single | 0.12±0.04 | 7.2±0.6 | 0.17±0.01 | 6.62±0.08 |
| Acto-S1+EGTA | ADP-AIF ₄ | 547 | Multiple ^a | 0.8±0.1 | 4.1±0.1 | N/A | N/A |
| Acto-S1+EGTA | ADP-BEFx | 780 | Single | 0.37±0.2 | 5.7±0.7 | 0.30±0.07 | 5.89±0.34 |
| Acto-S1+EGTA | ADP-AIF ₄ | 780 | Single | 0.41±0.16 | 5.5±0.6 | 0.23±0.02 | 6.24±0.12 |

^aIndicates multiple exponential fits performed by constraining additional components to the fits to both the 547 and 690 decays, so that only the fastest decaying component was extracted. By multiple fitting, the unbound donors signal is discarded and the shorter, fastest component corresponds to the bound molecules only. No multiple fitting was required for the tropomyosin data.

measurements (between bent and extended lever arm, Fig. 10) are corroborated by the chicken crystal structure differences of 6.6 nm – 5.1 nm = 1.5 nm and the scallop muscle myosin crystal structure differences of 1.4 nm (Root 2002b).

A

Pre-power stroke
transition state analogs



B

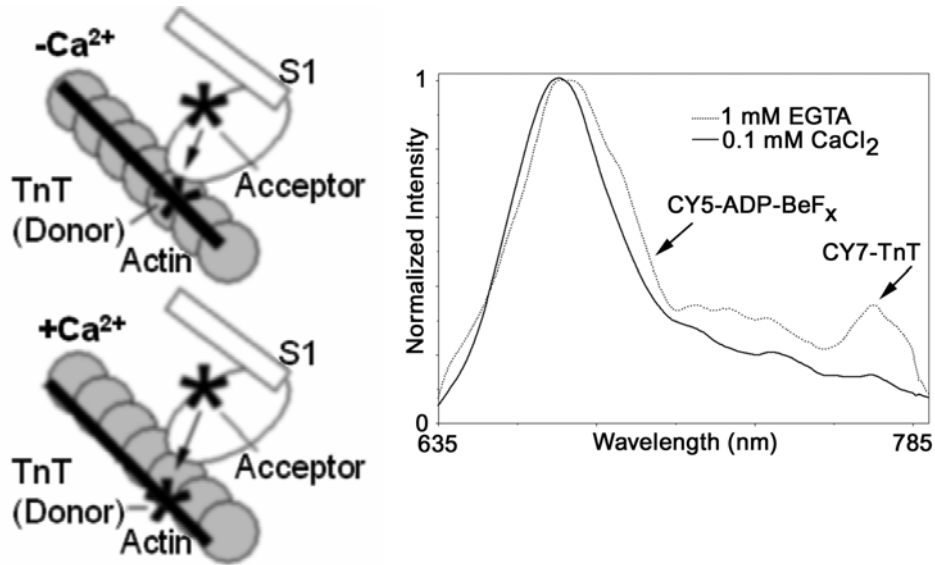


Fig. 10: Lever arm positions and calcium effect. Lever arm positions detected by nanocircuit illustrated using TnT labeled by Cy7 as second acceptor: bent lever arm or pre-power stroke and extended lever arm or post-power stroke. Also illustrated unbound molecules that will be detected by 547 nm emissions and not by 780 nm emissions, explaining the single and double exponential fitting of decays obtained at 547 nm. Extended versus bent S1 conformations estimated to be 1-1.5 nm in difference (A). Calcium induced thin filament structural changes detected by nanocircuit. RET between Cy5-ADP and Cy7-troponin T detects calcium induced changes between S1 and troponin T (B)

4.3 Calcium Induced Thin Filament Structural Changes Detected by Nanocircuit

Table 1 measurements indicate that the impact of calcium level is small on the RLC to nucleotide site distance. When using the nanocircuit with troponin T as the second acceptor, the measured separation distance of N terminus RLC to nucleotide binding site is 5.6 ± 0.6 nm and 5.5 ± 0.3 nm in the presence of calcium and transition state analogs beryllium as well as aluminum fluoride respectively, changing only to 5.7 ± 0.7 nm and 5.5 ± 0.6 nm (beryllium and aluminum fluoride respectively) upon addition of calcium-chelator EGTA at 1 mM concentration. The emission spectra collected (Fig. 10B), however, indicates that calcium does have an impact, indicated by a pronounced increase in the ratio of Cy7-troponin T sensitized emission relative to Cy5-ADP emission upon the addition of 1mM EGTA in the presence of aluminum or beryllium fluoride. The increased energy transfer observed between the Cy5-ADP and Cy7-troponin T sites could be due to a conformational change or orientation changes between the two dipoles when calcium is bound. Additionally, these results show that there are still bound S1 molecules after the removal of calcium which may presumably be weak binding interactions.

4.4 Post-Power Stroke Lever Arm Conformations Detected on Myosins Bound Close to Cy7-Tropomyosin α and Far Away From the Troponin Complex. Pre-power Stroke Conformations Detected on Myosins Bound Close to Cy7-Troponin T

Table 1 summarizes the distances measured using the nanocircuit on the lever arm positions of S1 molecules bound close to the troponin complex and bound along and between troponin complexes. Measurements of the nanocircuit using as second acceptor troponin T, indicate that the location of the binding of S1 relative to troponin T

influences the position of the lever arm. Depending on the proximity of S1 to troponinT, the sensitized emissions of Cy5-ADP and Cy7-TnT should differ. Table 1 shows that the calculated distance from the RLC to Cy5-ADP is $6.4 \text{ nm} \pm 0.4 \text{ nm}$ but when this distance is measured through the Cy7-TnT sensitized decay under identical conditions, the distance drops to $5.6 \pm 0.2 \text{ nm}$. These measurements suggest that when S1 binds near troponin T, the lever arm orients preferentially towards a pre-power stroke conformation, presumably due to steric hindrances; rather than in the more typical case, when it binds further away from troponin.

Measurements of the nanocircuit using as second acceptor tropomyosin labeled at the single Cys 190 of tropomyosin α with CY7, indicate a lever arm rotation of S1 molecules bound near tropomyosin and in between troponin complexes of distances that correspond to predominantly post-power stroke conformations in support to the present hypothesized model. Post-power stroke conformations are observed regardless of the presence of transition state analogues in S1's bound along and in between troponin complexes.

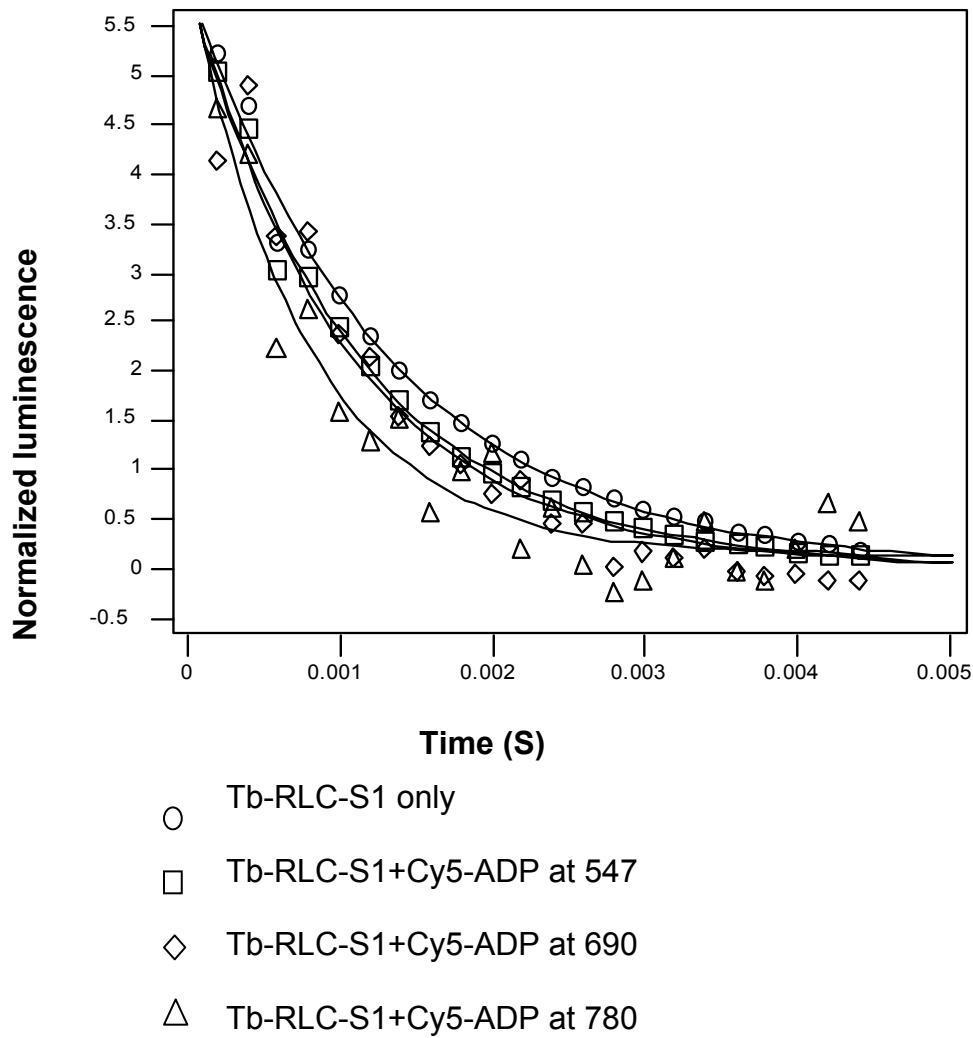


Fig. 11: Luminescence decay curves: Decay curves following excitation of CS124 in RLC with Last Acceptor Cy7-TnT. Measured in a luminescence spectrometer after excitation at 337 nm and estimated by single exponential curve fitting at 547, 690 and 780 nm. Lifetime of the donor changes as read at different emissions to isolate specific conformations of S1 lever arms along the thin filament. At emission 547 nm unbound and bound S1's detected. At emission 780 nm, only S1's bound close to troponin T are isolated.

CHAPTER 5

DISCUSSION

5.1 Steric Hindrance on Lever Arm Rotation Model: Myosins Bound Proximally to the Troponin Complex have a Lever Arm Biased towards Pre-Power Stroke State whereas Myosins Bound in between the Troponin Complex have Lever Arms in Post-Power Stroke States

The distances observed using the nanocircuit on the lever arm positions of S1 molecules bound close to the troponin complex indicate that the location of the binding of S1 relative to troponin T influences the position of the lever arm. This pre-power stroke positioning has been observed not only in the presence of the transition state analogs but in the presence of Cy5ADP alone. S1 binds near troponin T with lever arm positions preferentially towards a pre-power stroke conformation than when it binds further away from troponin, in between troponin complexes and near tropomyosin in which case the lever arm of S1 molecules situate preferentially at post-power stroke conformations. Measurements from the nanocircuit corroborate the data calculations done by triangulation measurements using FRET and computational docking that yield an atomic model of S1 bound to one side of the troponin complex with less steric hindrance when the lever arm is in a pre-power stroke orientation (Patel, *et al.*, 2005). Fig. 12 illustrates in schematic form this concept that based on the present study and the docking experiments, it is suggested that preferential different lever arm conformations are presumably due to steric hindrances.

The molecular docking experiments using LRET measurements were performed with various constrains from different sites of the myosin head to the same avian breast troponin T isoform as the one used in the present study (Patel, *et al.*, 2005). The troponin T isoform, has calcium binding properties that were discovered during its

characterization and a single cysteine (used for the attachment of probes) situated very close to the interface between the T, I and C subunits (Root and Jin, 2000). The nanocircuit results indicate the first of a two way effect that occurs during actomyosin interaction. First, the troponin T position in the thin filament affects the binding of S1 to a preferentially pre-power stroke state. Secondly, the triangulation measurements indicate that troponin influences the ability of S1 molecules to bind to specific locations along the thin filament because these RET measurements situate the troponin complex near loop 3 in the nearest myosin S1 bound to actin, therefore, modeling based on these measurements suggest myosin binds to one side of the troponin complex . Furthermore, molecular modeling docking indicates that the myosin must be in the pre-power stroke state to bind this close to troponin on actin (Patel, *et al.*, 2005 and Fig. 12).

Models of the actomyosin interface have been built using the x-ray structures of individual proteins and electron micrographs of actin filaments decorated by S1 (Rayment *et al.*, 1993b, Schroeder *et al.*, 1993), dynamic docking of actomyosin has also been observed with resonance energy transfer (Root *et al.*, 2002), as well as computational docking using molecular mechanics (Root, 2002a) to further define the important residues responsible for the acto-S1 interaction. Loop 3 of S1 has been defined as a secondary actin binding site of myosin, and has been shown in skeletal striated muscle myosins, in particular, to cross-link and therefore interact with actin via loop 3 (Van Dijk, 1999). The results correspond to all the above mentioned models of the actomyosin interface, and taking them all into consideration, the troponin label is predicted to be in very close proximity to loop 3 (Patel *et al.*, 2005).

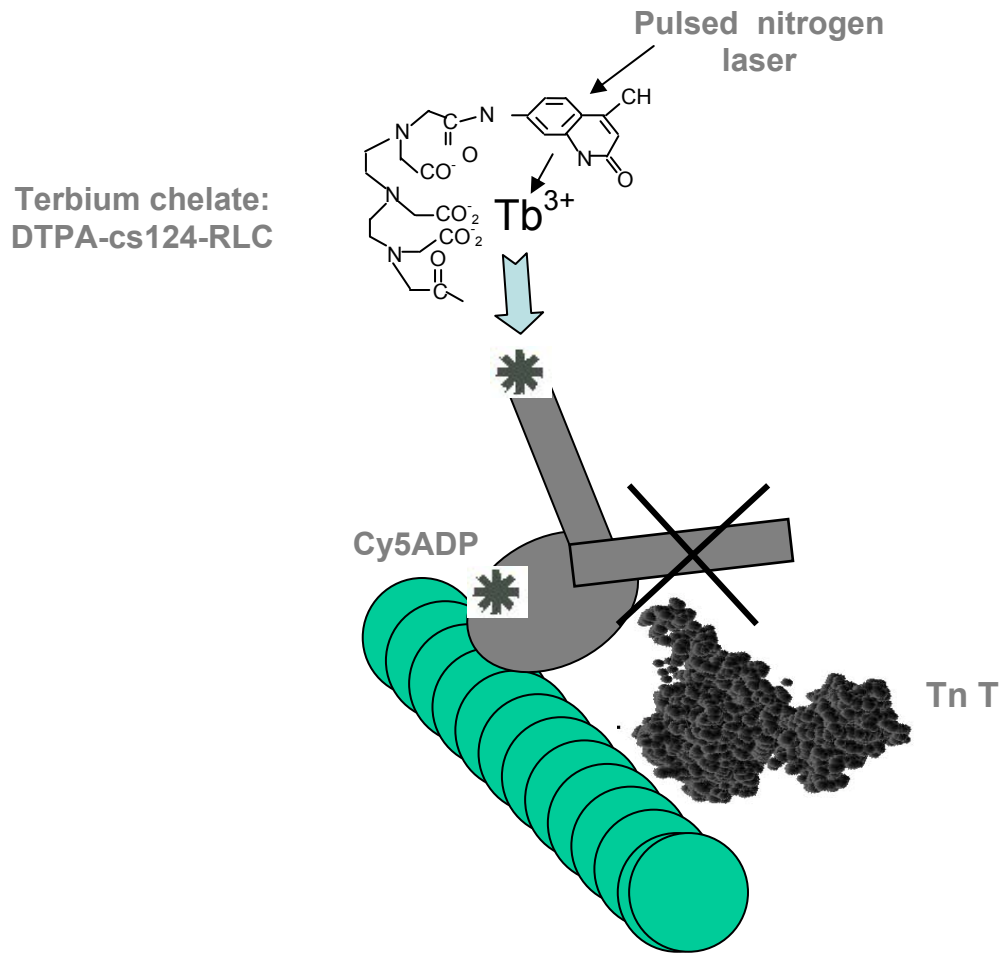


Fig. 12: Hindrance on lever arm rotation model. Myosins bound proximally to the troponin complex have a lever arm biased towards pre-power stroke state. Scheme based on the atomic model of troponin docking to actoS1 with less steric hindrance when the lever arm of myosin is in the pre-power stroke position.

5.2 What Value Does a Prevention of a Power Stroke near a Troponin Complex Have?

Interactions with or near loop 3 of myosin S1 with troponin T hint to the importance of this region for the regulation of the S1-actin contacts in skeletal muscle and cardiac systems, both of which are regulated via the troponin-tropomyosin system. A peptide antibody against the loop 3 region of skeletal muscle has been shown to inhibit the sliding velocity of actin filaments on in vitro motility assays (Blotnick *et al.*,

1995). Only the motor domains containing the loop 3 of skeletal muscle myosin have been shown to cross-link and therefore interact with actin, this interaction was not observed in smooth muscle or recombinant constructs of the slime mold *Dictyostelium* myosin II motor (Van Dijk *et al*, 1999). Additionally, only recombinant chimeric constructs of *Dictyostelium* myosin II motor domain where the loop 3 region had been substituted by the one of skeletal myosin showed significant actin cross-linking (Van Dijk *et al*, 1999). The lever arm region of S1 confers great flexibility to myosin and is primarily responsible for the changes in the sarcomere stretch that produces the sliding of thick and thin filaments. The S1 lever arm attaches to the thick filament backbone via subfragment-2 (S2); both regions are the heavy meromyosin product of trypsin digest. Although not as flexible as the lever arm, a second region of flexibility has been observed at the hinge connecting the S2 region and the light meromyosin (Gundapaneni *et al*, 2005). Furthermore, regulatory components spaced every 7 actin monomers in the form of the troponin complex may guide the binding positions of S1 molecules in the vicinity. The troponin complex preventing close S1 molecules from undergoing a power stroke could confer a limit to the sliding of thick filaments allowing enough flexibility (performed by the majority of S1 molecules that undergo a full power stroke) but ensuring the preservation of the elastic component to stop and recoil back. The loop 3 region of the actin-S1 interface, of close contact with troponin T, has been shown to have a modulating effect in the interaction with actin. The troponin complex may contribute to the modulating effect of nearby S1 molecules by inhibiting their power stroke and sequestering the lever arms in pre-power stroke positions. Experiments cross-linking of S1 to actin done in the presence of $Mg\cdot ADP\cdot ALF^{4-}$ have shown that the

area of loop 3 involved in the actomyosin interface is smaller than in the absence of nucleotide (Martin *et al.*, 2006), this observation corroborates why the troponin complex can fit better closer to S1 molecules that have a pre-power stroke positioned lever arm in the actomyosin interphase. A few periodically situated S1 molecules with lever arms unable to undergo a complete power stroke may create a limit or stop mechanism for further shortening. This mechanism can aid in the function of the giant protein titin that spans as a molecular scaffold of the sarcomere further serving as a molecular spring. Titin extends from the Z-line of the sarcomere to the M-band. Titin, the largest single polypeptide found in nature, provides binding sites for numerous proteins thus its importance for the assembly of the sarcomere. Several proteins important for the stability of the sarcomeric structure are found in the Z-line as well as in the M-band of the sarcomere. In the Z-line, titin binds to the thin filament system via the protein alpha-actinin. Therefore, both titin and the troponin complex components in the muscle fibers may cooperatively influence the recoiling after extension (due to contraction) with troponin behaving as an elastic limit while titin provides passive tension for optimal interaction of myofilaments and sarcomere length. Regulation of sarcomere length has been shown to be important for isometric tension, too long and too short lengths generate low force whereas intermediate lengths are optimal for tension and force generation in muscle. Experiments conducted in 1966 defined well this relationship based on the optimal overlapping of myosin and actin filaments to generate tension. If a sarcomere of length 3.65 μm (myosin filaments of 1.65 μm and actin filaments of 2 μm in length) is highly stretched to its limit, there would be no overlap between interdigitating actin and myosin filaments. Additionally, it has been observed that

sarcomere shortening below 2 μm results in great filament overlap but no tension generation, at this point, the bare zone of the myosin backbones devoided of S1 crossbridges does not allow cross-bridge connections to be made (Gordon *et al.*, 1966a; 1966b). Troponin T as well as the other subunits of the troponin complex are important and may also have effects in tension development. Experiments of partial extractions of the Ca^{2+} binding troponin C subunit in mammalian skinned muscle fibers, from which the sarcolemma has been removed, have evidenced the molecular cooperativity that exists between the other thin filament regulatory proteins. These experiments have shown that partial extraction of troponin C still results in the development of Ca^{2+} insensitive active tension evidencing the cooperativity of the other functional subunits of the thin filament (Moss *et al.*, 1986; Metzger and Moss, 1991). In a similar manner, it would be expected that partial extraction of troponin T in muscle fibers, would produce less uniform sarcomere lengths with shortening in support of the role of troponin T in influencing further shortening of the sarcomere by affecting the power stroke of nearby S1 bound cross-bridges.

5.3 Transition State Analogs Aluminum and Beryllium Fluoride behave similarly causing Pre-Power Stroke Conformations when Observed with Troponin T and Post-Power Stroke Conformations when Observed from Tropomyosin

Transition state analogs aluminum and beryllium fluoride were used in order to characterize and to isolate weak binding states or ADP-Pi of the ATPase cycle. As observed in previous studies, assigning a particular kinetic state to any of these analogs has proven difficult due to their properties being dependent on the assay conditions and the presence of other proteins in the

sarcomere. In this present case, the results have been very consistent. When used in the nanocircuit in solution and in conjunction with the labeled troponin T, they allowed the identification of pre- power stroke conformations and no difference was observed in the effects of both metallofluorides, these results are in concordance with the crystallographic results obtained with both analogs with smooth myosin S1 where no difference was observed in the use of either of them (Dominguez *et al.*, 1998). The use of transition state analogs in the tropomyosin labeled assay was not able to induce pre-power stroke conformations even after the reduction of calcium in bound molecules, reaffirming the selection of post-power stroke structures of most S1 molecules bound along tropomyosin. Not being able to force a pre-powerstroke conformation is not unusual since it has been observed that the presence of other contractile proteins may affect the state in which the lever arm is isolated using the analogs (Phan and Reisler, 1993). The present results show the greater number of S1 molecules that can undergo their complete power stroke while few S1 molecules situated with their loop 3 region close to troponin staying in the short lived pre-power stroke state.

5.4 Cooperativity of Activation

Calcium regulates contraction in striated muscle. As already mentioned, the thin filament is composed of actin arranged helically with regulatory proteins tropomyosin binding as a dimer to 7 actin monomers in the thin filament helix and the proteins of the troponin complex binding every 7 actin monomers as well. In the absence of calcium, troponin I binds to actin and to tropomyosin via troponin T. Troponin I also interacts with troponin C, the subunit that upon binding with Ca^{2+} causes the detachment of TnI to

actin allowing tropomyosin to move over the surface of the thin filament to expose weak and strong myosin binding sites and allowing the interaction of myosin S1 heads to actin. This interaction, allows the power stroke to occur causing contraction when thin filaments slide over thick filaments. This model of steric regulation has been observed consistently with electron micrographs and cryoelectron microscopy and helical image reconstruction of F-actin-troponin-tropomyosin complexes in the low Ca^{2+} and high Ca^{2+} states (Holmes, 1995; Xu, 1999). The nanocircuit results indicate that the prevention of a complete power stroke near the periodically occurring troponin complex still allows the recruiting of other S1 molecules for the subsequent cooperative activation of the thin filament, as complete power strokes have been extracted at wavelength 690 nm corresponding to S1 molecules bound but not necessarily close to the troponin complex. These results corroborate further studies done in skinned skeletal muscle fibers that had shown that complete activation of the thin filament by bound myosin cross-bridges requires not only the presence of calcium but also strong-binding myosin cross-bridges to actin in a cooperatively increasing manner (Lehrer, 1994; Gordon *et al.*, 2000)

5.5 Calcium Induced Thin Filament Structural Changes Detected by Nanocircuit.

The impact of calcium level in the lever arm position of the RLC to nucleotide site distance has been relatively small, in the presence of analogs and even upon addition of calcium-chelator EGTA at 1 mM concentration. The emission spectra collected (Fig. 10B), however, indicates that calcium does have an impact, indicated by a pronounced increase in the ratio of Cy7-troponin T sensitized emission relative to Cy5-ADP emission upon the addition of 1mM EGTA in the presence of aluminum or beryllium fluoride.

Increased energy transfer between the nucleotide site and troponin T in response to calcium provides additional information about the dynamics of the thin filaments. More may be observed in actual myofibrils where all thin filament proteins are present. Additionally, Figure 10B illustrates the displacement of the troponin complex relative to myosin reported by the changes in the sensitized emission in response to calcium quenching. A likely explanation of the increased energy transfer observed between the Cy5-ADP and Cy7-troponin T sites could be due to orientation changes between the two dipoles when calcium is bound. Aluminum fluoride has been shown in the past to increase the α -helicity and tyrosine fluorescence of Ca^{2+} binding troponin C (Phan and Reisler, 1993); the avian troponin T labeled with Cy7, naturally binds calcium and may be affected some by the phosphate analogs without necessarily affecting distances between the fluorophores.

5.6 Other Possible Applications of the Fluorescent Nanocircuit

The fluorescent nanocircuit can be applied to different systems to study biological questions involving different molecular ternary complexes. So far, triple FRET cascades have been used in synthetic dendrimers, single stranded DNA and RNA polymerase/DNA complexes using organic fluorophores (Serin *et al.*, 2002; Tong *et al.*, 2001; Lee *et al.*, 2006). However, the use of a three FRET relay system combined with lanthanides for greater precision, can be extended to the study of the interactions of triple stranded DNA, protein folding and to answer more complex interactions such as dynamic structural changes in solution involving proteins and protein/DNA complexes. Most significantly, the exploitation of the great time-resolution provided by the mixture of

slow lanthanide decays (ms) with fast conventional decays (ns) enables the construction of nanocircuits that can report structural changes in the rate-limiting (slow decaying) steps of the relay only in the presence of the terminal acceptor. Even in the presence of a small fraction of lanthanide donor and/or first acceptor (CY5) relative to the terminal acceptor (CY7), it is possible to precisely quantify the energy transfer in this first step (lanthanide to CY5) only when the terminal acceptor (CY7) is in close proximity. This degree of discrimination has only been reported with the time-resolved probes as used in the unique fluorescent nanocircuit described herein.

5.7 Conclusions

The goals of a newly developed spectroscopic nanocircuit were successfully accomplished. Not only did it allow the identification of different conformations of the lever arm by signal averaging from a large number of molecules, but it also permitted exploiting the signal of the last acceptor of the nanocircuit relay to identify the most critical conformations to a given transition kinetic step using phosphate analogs and in proximity to two different regulatory proteins of the thin filament: troponin and tropomyosin. The skeletal myosin lever arm exists in various orientations prior to the association of myosin to actin. Upon initial binding events with actin, pre-power stroke orientations are selected on S1 molecules bound close to the troponin complex the same ones that cannot complete their power stroke. S1 molecules bound along tropomyosin and in between troponin complexes on the other hand, are driven towards post-power stroke conformations upon phosphate release.

REFERENCES

- Bauer, C. B., Holden, H. M., Thoden, J. B., Smith, R., and Rayment, I. (2000). X-ray structures of the Apo and Mg-ATP-bound states of *Dictyostelium discoideum* myosin motor domain. *Journal of Biological Chemistry*, 275, 38494-38499
- Bigay, J., Deterre, P., Pfister, C., and Chabre, M. (1987). Fluoride complexes of aluminum or beryllium act on G-proteins as reversible bound analogues of the gamma phosphate of GTP. *EMBO Journal*, 6, 2907-2913
- Blotnick, E., Miller, C., Groschel-Stewart, U., and Muhlrad, A. (1995). Immunochemical probing of the functional role of the 238-246 and 567-574 sequences of myosin heavy chain. *European Journal of Biochemistry*, 232, 235-240
- Chabre, M. (1990). Aluminofluoride and beryllifluoride complexes: new phosphate analogs in enzymology. *Trends in Biochemical Sciences*, 15, 6-10
- Colowick, S. and Kaplan, N. (1982). Structural and contractile proteins. The contractile apparatus and the cytoskeleton. *Methods in Enzymology*, 85, 234-259
- Cooke, R. (1986). The mechanisms of muscle contraction. *Critical Reviews in Biochemistry*, 21, 53-118
- Dominguez, R., Freyzon, Y., Tybus, K.M., and Cohen, C. (1998). Crystal structure of a vertebrate smooth muscle myosin motor domain and its complex with the essential light chain: visualization of the pre-power stroke state. *Cell*, 94, 559-571
- Ebashi, S. and Endo, M. (1968). Calcium ion and muscle contraction. *Progress in Biophysics and Molecular Biology*, 18, 123-183
- Ebashi, S., Endo, M. and Otsuki, I. (1969). Control of muscle contraction. *Quarterly Review of Biophysics*, 2, 351-384
- Fisher, A. J., Smith, C. A., Thoden, J. B., Smith, R., Sutoh, K., Holden, H. M. and Rayment, I. (1995). X-ray structures of the myosin motor domain of *Dictyostelium discoideum* complexed with MgADPBeF_x and MgADPAIF₄. *Biochemistry*, 34, 8960-8972
- Getz, Elise Burmeister, Cooke, Roger and Selvin Paul R. (1998). Luminescence resonance energy transfer measurements in myosin. *Biophysical Journal*, 74, 2451-2458
- Gordon, A.M., Huxley, A.F., and Julian, F.J. (1966). Tension development in highly stretched vertebrate muscle fibres. *Journal of Physiology*, 184, 143-169

- Gordon, A.M., Huxley, A.F., and Julian, F.J. (1966). The variation in isometric tension with sarcomere length in vertebrate muscle fibres. *Journal of Physiology*, 184, 170-192
- Gordon, A.M., Homsher, E., and Regnier, M. (2000). Regulation of contraction in striated muscle. *Physiological Reviews*, 80, 853-924
- Gulick, A. M., Bauer, C. B., Thoden, J. B., Pate, E., Yount, R. G., and Rayment, I. (2000). X- ray structures of the *Dictyostelium discoideum* myosin motor domain with six non-nucleotide analogs. *Journal of Biological Chemistry*, 275, 398-408
- Gundapaneni, D., Xu, J., and Root, D.D. (2004). High flexibility of the actomyosin crossbridge resides in the skeletal myosin subfragment-2 as demonstrated by a new single molecule assay. *Journal of Structural Biology*, 149, 117-126
- Holmes, K.C. (1995). The actomyosin interaction and its control by tropomyosin. *Biophysical Journal*, 68, 2-7
- Holmes, K. C. (1997). The swinging lever-arm hypothesis of muscle contraction. *Current Biology*, 7, 112-118
- Houdusse, A., Kalabokis, V.N., Himmel, D., Szent-Györgyi, A.G., and Cohen, C. (1999). Atomic structure of scallop myosin subfragment S1 complexed with MgADP: A novel conformation of the myosin head. *Cell*, 97, 459-470
- Houdusse, A., Szent-Györgyi, A.G., and Cohen, C. (2000). Three conformational states of scallop myosin S1. *Proceedings of the National Academy of Sciences USA*, 97, 11238-11243
- Jin, J.P., and Root, D.D. (2000). Modulation of troponin T molecular conformation and flexibility by metal ion binding to the NH₂-terminal variable region. *Biochemistry*, 39, 11702-11713
- Kraft, T., Mählmann, E., Mattei, T., and Brenner B. (2005). Initiation of the power stroke in muscle: Insights from the phosphate analog AIF₄. *Proceedings of the National Academy of Sciences USA*, 102, 13861–13866
- Lee, N.K., Kapanidis, A.N., Koh, H.R., Korlann, Y., Ho, S.O., Kim, Y., Gassman, N., Kim, S.K., Weiss, S. (2006). Three-color alternating-laser excitation of single molecules: Monitoring multiple interactions and distances. *Biophysical Journal*, Oct 13; (E-pub ahead of print)
- Lehrer, S.S. (1994). The regulatory switch of the muscle thin filament: Ca²⁺ or myosin heads. *Journal of Muscle Research and Cell Motility*, 15, 232-236
- Martin, B., Karczewska, E., and Plitszka, B. (2006). Effect of nucleotide on interaction of the 567-578 segment of myosin heavy chain with actin. *Biochimica et Biophysica Acta*, 1764, 217-222

- Maruta, S., Henry, G.D., Sykes, B.D., and Ikebe, M. (1993). Formation of the stable myosin-ADP-aluminum fluoride and myosin-ADP-beryllium fluoride complexes and their analysis using ^{19}F NMR. *Journal of Biological Chemistry*, 268, 7093-7100
- Metzger, J.M., and Moss, R.L. (1991). Kinetics of a Ca^{2+} -sensitive cross-bridge state transition in skeletal muscle fibers. *Journal of General Physiology*, 98, 233-248
- Moss, R.L., Allen, J.D., and Greaser, M.L. (1986). Effects of partial extraction of troponin complex upon the tension-pCa relation in rabbit skeletal muscle. *Journal of General Physiology*, 87, 761-774
- Nikolaeva O.P, Dedova I.V, Khvorova I.S, and Levitsky D.I. (1994). Interaction of F-actin with phosphate analogues studied by differential scanning calorimetry. *FEBS Letters*, 351, 15-18.
- Patel, D., Coffee, P., and Root, D.D. (2005). The structural relationship of muscle myosin to thin filament regulatory proteins. *Gordon Summer Research Conference Abstract*
- Perry, S. (2001). Vertebrate tropomyosin: Distribution, properties and function. *Journal of Muscle Research and Cell Motility*, 22, 5-49
- Peyser, Y.M., Ajtai, K, Burghardt, T.P. and Muhlrade, A. (2001). Effect of ionic strength on the conformation of myosin subfragment 1-nucleotide complexes. *Biophysical Journal*, 81, 1101–1114
- Phan, B., and Reisler, E. (1992). Inhibition of myosin ATPase by beryllium fluoride. *Biochemistry*, 31, 4787-4793
- Phan, B., and Reisler, E. (1993). Aluminum fluoride interactions with troponin C. *Biophysical Journal*, 65, 2511-2516
- Rayment, I; Rypniewski, W.R; Schmidt-Bäse, K., Smith, R., Tomchick, D. R., Benning, M. M., Winkelmann, D. A., Wesenberg, G., and Holden, H. M. (1993a). Three-dimensional structure of myosin subfragment-1: A molecular motor. *Science*, 261, 50-58
- Rayment, I., Holden H.M., Whittaker, M., Yohn, C.B., Lorenz, M., Holmes, K.C., and Milligan, R.A. (1993b). Structure of the actin-myosin complex and its implications for muscle contraction. *Science*, 261, 58-65
- Root, D.D. (2002a). A computational comparison of the atomic models of the actomyosin interface. *Cell Biochemistry and Biophysics*, 37, 97-110
- Root, D.D. (2002b). The dance of actin and myosin. A structural perspective. *Cell Biochemistry and Biophysics*, 37, 111-139

- Schroeder, R.R, Manstein, D.J., Jahn, W., Holden, H., Rayment, I., Holmes K.C., and Spudich J.A. (1993). Three-dimensional atomic model of F-actin decorated with *Dictyostelium* myosin S1. *Nature*, 364, 171-174
- Serin, J.M., Brousmiche, J.M., and Frechet, J. (2002). Cascade energy transfer in a conformationally mobile multichromophoric dendrimer. *Chemical Communications*, 22, 2605-2607
- Smith, C.A. and Rayment, I. (1996). X-ray structure of the magnesium(II).ADP.vanadate complex of the *Dictyostelium discoideum* myosin motor domain to 1.9 Å resolution. *Biochemistry*, 35, 5404-5417
- Smyczynski, C. and Kasprzak, A. A. (1997). Effect on nucleotides and actin on the orientation of the light chain-binding domain in myosin subfragment 1. *Biochemistry*, 36(43), 13201-13207
- Sprang, SR. (1997). G protein mechanisms: insights from structural analysis. *Annual Review of Biochemistry* 66, 639-678
- Sternweis, P.C., and Gilman, A.G. (1982). Aluminum: A requirement for activation of the regulatory component of adenylate cyclase by fluoride. *Proceedings of the National Academy of Sciences USA*, 79, 4888–4891
- Takeda, S., Yamashita, A., Maeda, K., and Maéda Y. (2003). Structure of the core domain of human cardiac troponin in the Ca^{2+} saturated form. *Nature* 424, 35–41
- Tong, A.K., Jockusch, S., Li, Z., Zhu, H.-R., Akins, D.L., Turro, N.J., and Ju, J. (2001). Triple fluorescence energy transfer in covalently trichromophore-labeled DNA. *Journal of the American Chemical Society*, 123, 12923-12924
- Van Dijk, J., Furch, M., LaFont, C., Manstein, D., and Chaussepied, P. (1999). Functional characterization of the secondary actin binding site of myosin II. *Biochemistry*, 38, 15078-15085
- Vinogradova, M., Stone, D., Malanina, G., Karatzaferi, C., Cooke, R., Mendelson, R. and Fletterick, R. (2005). Ca^{2+} -regulated structural changes in troponin. *Proceedings of the National Academy of Sciences USA*, 102, 5038–5043
- Werber, M.M., Peyser, Y.M., and Muhlrads, A. (1992). Characterization of stable beryllium fluoride, aluminum fluoride, and vanadate containing myosin subfragment 1-nucleotide complexes. *Biochemistry*, 31, 7190-7197
- Xu, C., Craig, R., Tobacman, L., Horowitz, R., and Lehman, W. (1999). Tropomyosin positions in regulated thin filaments revealed by cryoelectron microscopy. *Biophysical Journal*, 77, 985-992

- Xu, J and Root, D.D. (1998). Domain motion between the regulatory light chain and the nucleotide site in skeletal myosin. *Journal of Structural Biology* 123, 150-161
- Xu, J and Root, D.D. (2000). Conformational selection during weak binding at the actin and myosin interface. *Biophysical Journal*, 79, 1498-1510
- Zhang, Z., Jin, J.P., Root, D.D. (2004). Binding of calcium ions to an avian flight muscle troponin T. *Biochemistry*, 43, 2645-2655.